Neutron Diffraction from Single Crystals

11

11.1 Introduction

When we discussed the variation of observable symmetry according to the nature of the examining probe, Sect. 1.4, we stated that one possible probe is a neutron beam. As an example, when the structure of elemental chromium is examined by X-ray diffraction, it shows a body-centered cubic arrangement, Fig. 11.1a. Elemental chromium has the electronic configuration (Ar $3d^5$ $4s^1$); it is antiferromagnetic at room temperature, and its electron spins, arising from the unpaired electrons, give rise to the *magnetic* structure shown in Fig. 11.1b. The magnetic moment of the neutron interacts with the permanent dipole of chromium to form this structure, and consequently the diffraction record shows a primitive cubic structure.

Neutron diffraction can distinguish between isotopes, aid the study of alloy systems, such as the Cu–Zn phases (similar atomic numbers) and magnetically ordered structures, and reveal the presence of light atoms in the presence of heavy atoms, such as hydrogen in sodium hydride—a difficult matter with X-rays.

As an example of the detection of hydrogen atoms, we cite the structure of potassium dihydrogen phosphate, KH_2PO_4. Hydrogen atoms scatter neutrons strongly, but because the scattering cross section (q.v.) is negative, the nuclear density contours are also negative for this atom; it also produces a high background owing to incoherent scattering. Deuterium, however, has a large, positive coherent scattering with only small background. Thus, it is common practice to replace hydrogen by deuterium in neutron diffraction studies of hydrogen atom positions in crystal structures. Notable examples of this application are the precise location of the deuterium (hydrogen) atom positions in potassium dihydrogen phosphate, KH_2PO_4, Fig. 11.2, and sucrose, $C_{12}H_{22}O_{11}$.

Neutron diffraction is also an important and powerful technique used in combination with X-ray diffraction for locating hydrogen atoms or protons in both small molecules and macromolecules. For example, neutron scattering has been used in protein crystallography to distinguish between the side chain C=O oxygen atom and the NH_2 nitrogen atom in asparagine and glutamine residues because of the significant difference between the neutron scattering lengths of oxygen and nitrogen: this distinction is difficult to achieve with X-ray diffraction. It is also possible to distinguish between N–H and C–H groups on histidine rings (q.v.). In both cases the proper positioning of these groups is an important factor in the understanding of the biological action of the protein; see also Sect. 9.4.3. It is also possible to ascertain whether a given nitrogen atom is protonated (deuterated) or unprotonated, an ambiguity which again may be difficult to resolve by other means [1].

M. Ladd and R. Palmer, *Structure Determination by X-ray Crystallography: Analysis by X-rays and Neutrons*, DOI 10.1007/978-1-4614-3954-7_11,

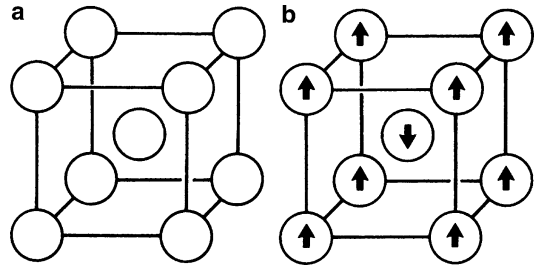

Fig. 11.1 Unit cell of the crystal structure of elemental chromium. (**a**) By X-rays: body-centred cubic. (**b**) By neutrons: primitive cubic. The arrows represent the magnetic moment vector directions in the metal atoms

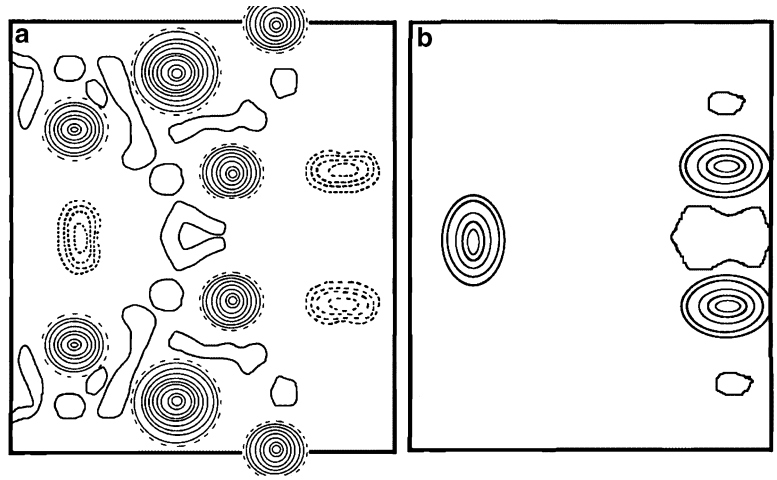

Fig. 11.2 Projections onto the x,y plane of the neutron scattering density for deuterated potassium dihydrogen phosphate, KD_2PO_4, in the room temperature tetragonal structure. (**a**) Direct synthesis, showing all atoms in the structure; the most intense peaks arise from the K and P atoms, which are superimposed in this projection. The other peaks are O atoms (full lines) and D atoms (dashed lines, indicating the negative scattering amplitude of this species). (**b**) Corresponding difference synthesis, in which only the D atoms appear. It is noteworthy that the diffraction ripples (series termination errors) around the heavy-atom positions in (**a**) are subtracted out in (**b**), so that the contours of D are free from the distorting effects of the ripples

11.1.1 Refinement of Hydrogen Atom Positions

The neutron diffraction results for sucrose give the value 1.09 Å for the C–H bond length, whereas by X-rays it is shown to be 0.98 Å; the corresponding O–H bond length values are 0.98 and 0.80 Å. These results are of interest in connection with the refinement of a structure. If the hydrogen atoms are included in the calculations but are not themselves refined, a not uncommon procedure, then with X-ray data it is reasonable to constrain the C–H bond length to be about 0.98 Å rather than 1.09 Å. The polarity of the C–H bond leads to a displacement of the electron density of hydrogen toward the carbon atom. Thus, the position of the electron density maximum for the hydrogen atom will not coincide with that given by neutron diffraction.

Neutron diffraction investigations can also be carried out on powdered crystalline samples, and we address this topic in Chap. 12. We proceed next to discuss neutron diffraction in detail and to give examples of structures determined by neutron crystallography.

11.2 Neutrons, Neutron Sources, and Data Collection

11.2.1 Neutrons

In 1923, some years after the historical Laue experiment, de Broglie introduced the wave-particle duality theory, which proposed that every material particle can behave also as a non-electromagnetic wave, opposed to the electromagnetic waves which include X-rays, light, and other types of wave phenomena such as heat and sound. According to de Broglie's theory, the particle wavelength λ is given by:

$$\lambda = h/p = h/mv \tag{11.1}$$

where h is the Planck constant and p, m, and v are, respectively, the momentum, mass, and speed of the particle.

Neutrons are sub-atomic particles which are bound to most atomic nuclei. A neutron has no net electric charge and a mass slightly greater than that of a proton. The number of protons in a nucleus is numerically equal to the atomic number and defines the type of the element. The number of neutrons determines the isotope of the element. For example, the abundant ^{12}C isotope has six protons and six neutrons, while the rare radioactive ^{14}C isotope has six protons and eight neutrons. While bound neutrons in stable nuclei are stable, free neutrons are unstable and undergo β-decay with a mean lifetime of just under 15 min. The nucleus of deuterium (heavy hydrogen) contains one proton and one neutron, whereas the hydrogen nucleus contains just one proton. This distinction has an important consequence in some neutron diffraction experiments, as we shall see.

11.2.2 Neutron Sources

Free neutrons are produced in both nuclear fission and fusion processes. Thus, large dedicated neutron sources are either nuclear fission reactors, or high flux spallation sources in which protons have been accelerated to high energies and directed on to a target so as to produce free neutrons. Spallation describes what happens when a high-energy proton is accelerated into a heavy target: a number of spallation particles, including neutrons, are produced. For every proton striking the nucleus, twenty to thirty neutrons are expelled. Meson production limits spallation efficiency above 140 MeV. At the 1 GeV proton energy level, the Spallation Neutron Source, Sect. 11.4.2, requires 30 MeV per neutron produced. All of these sources produce neutron beams that are useful in neutron diffraction experiments. Inside a reactor, thermal neutrons have an average energy corresponding to 308 K (35 °C), but there is actually a Boltzmann distribution of neutron energies, so that the emerging beam will have a range of energies (or temperature) and, more importantly, a range of wavelengths, according to (11.1). Hence an essentially "white" beam of neutron wavelengths is available, which can be limited, if required, to a desired wavelength range.

11.2.3 Neutron Data Collection

Monochromatic Neutron Data Collection

This method of data collection as the title suggests involves the isolation of a single neutron wavelength or limited range of wavelengths using suitable filters, corresponding closely to the use

of monochromatic X-radiation discussed in Sect. 3.1.4. Thus, when a beam of neutrons emanating from a reactor is slowed down and selected properly, wavelengths appropriate for crystal diffraction experiments can be produced. However, these processes cause the neutron beam to be significantly depleted in intensity, which has the over-riding consequence of prolonging data collection times to the unmanageable proportions of days or weeks. As a result, alternative methods of data collection have been developed.

Laue Diffraction Neutron Data Collection

In this now commonly used technique, a white neutron beam is used to produce Laue diffraction photographs or image records [2], Sect. 5.4.1ff, that can be processed to create a neutron intensity data set. This approach allows the full incident intensity of the neutron beam to be used without the use of filters, which enables data to be collected far more rapidly.

Monochromatic versus Laue Diffraction Neutron Data Collection

It is of interest to compare these two methods of data collection. In particular, what are the limits to data set completeness imposed by a Laue experiment vs. those of monochromatic data collection?

These methods of data collection are common to both X-ray and neutron diffraction techniques. Rigorous theoretical considerations [3, 4] have laid the foundations of Laue data collection, which, with the complications inherent in the method imposed by a lack of direct knowledge of the wavelength associated with a given diffraction intensity, initially seemed to be an unlikely method of successful data collection. From the Bragg equation, when a crystal diffracts a polychromatic beam of X-rays or neutrons, many orders of each Bragg reflection, hkl, $2h,2k,2l,\ldots$, may occur simultaneously and overlap exactly in scattering angle. The overlap of these multiple orders along a ray, a central line in reciprocal space, poses a problem for Laue methods. It has been shown [3] that:

1. More than 83% of all Bragg reflections occur on single rays when experimental values of λ_{max} and λ_{min} are used.
2. This proportion depends only on the ratio of λ_{max} to λ_{min} and not on the space group, unit-cell dimensions, crystal orientation, or the limiting resolution of the crystal, d^*_{max}, provided d^*_{max} is less than $2/\lambda_{max}$.
3. The total number of single rays, like the total number of all stimulated Bragg reflections, is approximately proportional to the wavelength range.
4. The proportion of reflections at a given resolution d^* that lie on single or double rays depends markedly on d^*, and on the ratio of λ_{max} to λ_{min}—it is generally lower at low resolution than at high.
5. Restricted angular acceptance of the detector can reduce significantly both the proportion and the total number of single rays.
6. Agreement between the theoretical distributions and those derived from analysis of X-ray Laue photographs of macromolecular crystals, and from extensive computer simulations, is good.

It is evident that, under a wide variety of experimental conditions, the effect of multiple orders is not a serious limitation on the use of the Laue method for structure determination. An analysis has also been presented [4] of the angular distribution of reflections in Laue diffraction, with particular application to the spatial overlap problem in synchrotron macromolecular crystallography. This shows the factors that govern the spatial overlap of spots and indicates tactics for experimental design. The analysis is also relevant to polychromatic neutron diffraction. These considerations have led to the development of both hardware and software [5] for Laue diffraction which has now come to be accepted as a standard collection method capable of producing data of high quality, completeness, and resolution for both X-ray and neutron diffraction from single crystals.

Time-Resolved Laue Neutron Diffraction Data Collection Using a Spallation Source
This is a third method of neutron data collection currently undergoing intense development. Neutrons are produced in a spallation source by bombarding a metal target with protons from a particle accelerator or synchrotron. Essentially each neutron from a spallation source can be assigned its own wavelength. Data collection by this method is analogous to carrying out hundreds of monochromatic experiments simultaneously. Further details on this type of experiment are given in Sect. 11.4.

11.2.4 Thermal Neutrons

The term "thermal neutron" is used to describe any free neutron that has been ejected from an atomic nucleus and has kinetic energy corresponding to the average energy of the particles at 308 K. Thermal neutrons are produced by slowing down more energetic atomic neutrons by passing them through a moderator. The neutron wavelength can be calculated from a consideration of its kinetic energy E:

$$E = \tfrac{1}{2} m_{\mathrm{n}} v^2 = kT \tag{11.2}$$

where m_{n} is the neutron mass and v its speed; k is the Boltzmann constant and T the absolute temperature. It follows that

$$v = (2kT/m_{\mathrm{n}})^{1/2}$$

and since $mv = p = (2kTm_{\mathrm{n}})^{1/2}$,

$$\lambda = h/p = A/T^{1/2} \tag{11.3}$$

where $A = h/(2km_{\mathrm{n}})^{1/2}$ and is a constant for a given particle type such as neutrons. Since m_{n}=1.6749 $\times\ 10^{-27}$ kg, $A = 3.0810 \times 10^{-9}$ m $\mathrm{K}^{1/2}$; hence, at 308 K

$$\lambda = 1.756 \times 10^{-10}\,\mathrm{m} = 1.756\,\text{Å} \tag{11.4}$$

This wavelength is suitable for crystal diffraction measurements. Since the neutron beam may be designed to comprise a range of wavelengths, the diffraction data are then processed using a Laue procedure, as referred to in Sect. 11.2. As in contemporary X-ray diffraction experiments, the sample may be flash frozen in order to prevent decomposition in the neutron beam and thus enable a full set of diffraction data to be collected on a single crystal sample.

11.3 Neutron Scattering

Whereas the scattering of X-rays increases with increasing atomic number and decreases with $\sin\theta$ for a given wavelength, neutron scattering factors, *scattering lengths*, do not depend on atomic number in any regular manner. One important difference from X-ray diffraction is that the hydrogen scattering length is comparable to those of other atoms, but of negative sign. This means that for hydrogen, ^{1}H, the beam scattered by the nucleus differs in phase by 180° from the scattering from a nucleus in the same position that has a positive scattering factor. However, deuterium, ^{2}H, has a positive neutron scattering length that is comparable in magnitude to that of hydrogen. Consequently,

Table 11.1 Neutron scattering lengths for common elements

Atom	Atomic number	Scattering length (fm)
H	1	−3.739
D	2	6.671
N	7	9.360
O	8	5.803
F	9	5.650
S	16	2.847

it is frequently a useful option to replace hydrogen with deuterium, that is, to deuterate crystal samples prior to neutron diffraction data collection in order to render positive the subsequent neutron density at these sites. In that way, they are easier to handle, for example, when using molecular graphics. This is not always possible if the sample is unstable. It should also be noted that in general all C–H hydrogen atoms are not exchangeable in the deuteration process. Because neutron scattering for hydrogen or deuterium is comparable in magnitude with that from other atoms, it is not so easy to classify atoms as "light" or "heavy" as we have done for X-ray diffraction, and this introduces a technical difficulty in the actual solving of crystal structures ab initio from neutron diffraction data. An advantage, however, is afforded by the use of ^{2}H over ^{1}H, that is a much lower associated background scattering level, because the incoherent scattering cross section of ^{2}H is about 40 times less than that of ^{1}H. Thus, the signal-noise ratio is greatly enhanced in neutron diffraction data measured from deuterated samples [6].

We have assumed tacitly that the number of *hkl* data is the same for both X-ray and neutron diffraction. Usually, neutron data sets are less extensive than their X-ray counterparts, and this serves to exaggerate still further these problems. It is therefore almost always necessary to solve a crystal structure initially from X-ray data, and subsequently to use this structure as a basis for a detailed neutron analysis, as has been done with the three examples of varying structural complexity given later in this chapter.

11.3.1 Neutron Scattering Lengths

Neutron scattering lengths for different atoms can be obtained from various sources including the website of the National Institute of Standards and Technology [7, 8]. Examples of scattering length data incorporated into the SHELX program suite [9] for the atoms H, D, N, O, F, and S are listed in Table 11.1.

11.4 Experimental Neutron Diffraction Data Collection

The practical use of neutron diffraction requires access to highly specialized neutron sources. These installations are purpose built to cater for a variety of neutron physics applications, in the same way as synchrotron installations are designed not only for X-ray diffraction, but can accommodate a wide range of studies from Raman spectroscopy to circular dichroism studies, for example. A list of neutron sources available to scientists on a global scale can be found at the end of this chapter. For present purposes, experimental arrangements that are available at two of these installations will be described in some detail.

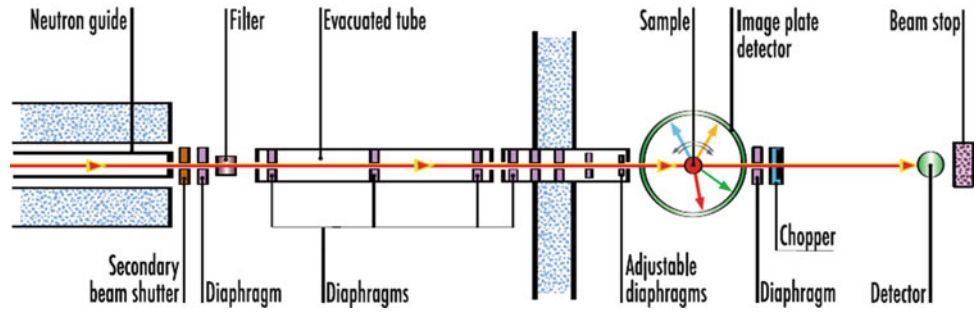

Fig. 11.3 Diagrammatic layout of the ultra-high speed VIVALDI neutron diffractometer (reproduced from the "yellow book" by courtesy of the Institut Laue-Langevin, Grenoble)

11.4.1 LADI-III and VIVALDI at ILL, Grenoble

At the Institut Laue-Langevin (ILL), the Laue diffraction instrument LADI-III produces extremely high-quality diffraction data. It employs a quasi-white cold-neutron beam with a large-area cylindrical detector based on neutron image plates and is used mainly for single crystal studies of relatively small proteins at medium or high resolution with the objective of locating individual hydrogen atoms in compounds of special interest, water molecules, or small ligands that can be deuterated to improve their scattering power. Good data sets from macromolecular structures that tend to have relatively weak scattering are measured routinely on this instrument. Protein crystals with unit-cell dimensions up to about 150 Å are accommodated and sample sizes can be as small as 0.1–0.2 mm^3.

The facility VIVALDI, Fig. 11.3, (Very-Intense Vertical-Axis Laue Diffractometer) [10, 11] was set up for use in 2001. This instrument allows large volumes of reciprocal space to be surveyed very quickly using an image-plate photographic Laue technique with a white neutron beam. Figure 11.4 is an example of a neutron Laue frame taken on VIVALDI. As well as single crystal analysis, it can accommodate applications for magnetism, nuclear charge-density waves, high-pressure studies, and structural phase transitions and allows rapid preliminary investigation of new materials even when only small single crystals are available. VIVALDI uses a technique similar to that of LADI-III, but employs a thermal neutron beam and is very well suited to fast data collection for crystal structures with smaller unit cells. Both VIVALDI and LADI-III have the detector cylinder axis vertical. In the case of VIVALDI, this facilitates acceptance of an "Orange" cryostat, and in both installations, the image plates are mounted and read on the inside of the cylinder in order to improve the detection efficiency. Consequently with VIVALDI, it is now possible to study larger biological complexes using smaller crystals than was previously possible [12]. As on LADI, the neutron-sensitive plates are based on the BaFBr storage-phosphor doped with Eu(II) ions, which is also used for X-ray image plates, Sects. 5.7.3 and 12.4.2, but with Gd_2O_3 added. The gadolinium nuclei act as neutron scintillators by creating a cascade of γ-rays and conversion electrons: an electron is released from the atomic shell by transferring the energy of a γ-quantum emitted from the same nucleus to its electron. Its kinetic energy is equal to the energy of the γ-quantum reduced by the binding energy of the electron.

The full thermal spectrum can be accepted without detrimental overlap of reflections for primitive unit cells up to 25 Å edge length. An optional filter based on multilayer super-mirrors can be placed upstream to deflect wavelengths longer than 3 Å which would otherwise contribute primarily to the background. A time-of-flight spectrum analyzer is located downstream to monitor changes in the wavelength. The entire instrument pivots on air cushions around the filter to allow selection of

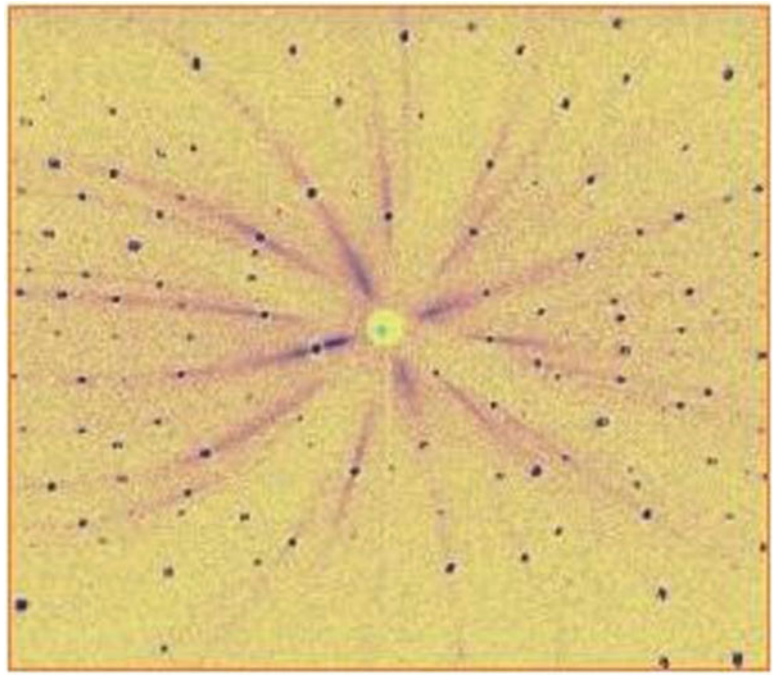

Fig. 11.4 A neutron Laue diffraction frame

wavelengths shorter than 3 Å, wavelengths longer than 3 Å, or the unfiltered beam. The beam size used is up to 10 × 10 mm^2 with a flux (unfiltered) of 10^9 neutron cm^{-2} s^{-1}.

The Orange cryostat can be used to select a sample temperature in the range 1.5–300 K. A typical experiment produces a small number of stationary-crystal, stationary-detector Laue diffraction patterns, distinguished by means of 20–30° rotations of the crystal about the vertical axis. The Laue data-analysis software developed on LADI from the CCP4 suite (see Appendix D) is used to produce the final data set for subsequent analysis.

Although VIVALDI was unparalled in data collection speed when it was introduced in 2001, it is now even faster. This has been brought about partly through the introduction of the more efficient Fuji "Niimura Special" white image plates, the replacement of some sections of the neutron guide by super-mirror guides, and a guide realignment, resulting in about three times as much neutron flux at the sample. Overall there has been a ninefold gain in efficiency. A short video showing the instrument set and each stage of the measurement of a neutron diffraction pattern is available on the ILL website [13].

11.4.2 Oak Ridge National Laboratory (ORNL) [14]

The High Flux Isotope Reactor (HFIR) and the HB-3A Diffractometer

Operating at 85 MW, HFIR is the highest flux reactor-based source of neutrons for research in the United States, and it provides one of the highest steady-state neutron fluxes of any research reactor in the world. The thermal and cold neutrons produced by HFIR are used to study physics, chemistry, materials science, engineering, and biology. The intense neutron flux, constant power density, and constant-length fuel cycles are used by more than 200 researchers each year for neutron scattering research into the fundamental properties of condensed matter.

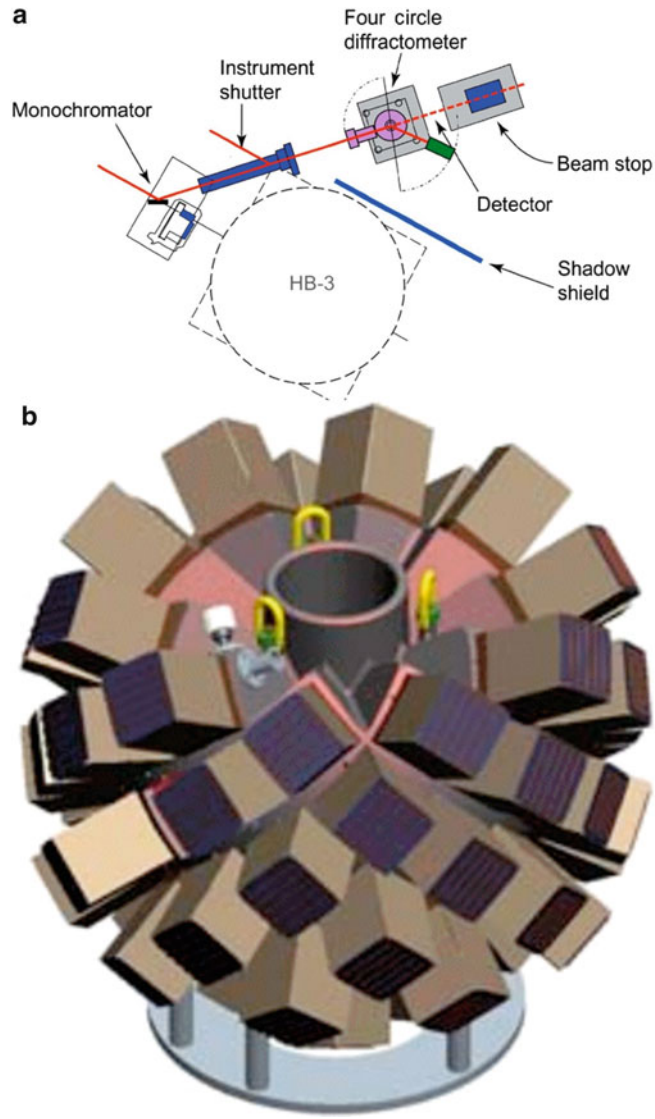

Fig. 11.5 (**a**) The HB-3A neutron single crystal diffractometer at ORNL, Tennessee (reproduced by courtesy of Dr Cao Huibo, ORNL, Tennessee.) (**b**) Detector array for the MaNDi instrument. The detectors are designed to cover a large solid-angle to record most of the neutrons scattered from a single crystal sample regardless of the reflection angle. The instrument design accommodates this by situating detectors approximately spherically around the sample

For single crystal diffraction studies, a four-circle diffractometer installation, the HB-3A, Fig. 11.5a, is available; see Sect. 5.6ff. The Huber goniometer has a full χ-circle with a 10 K closed-cycle helium refrigerator. The detector is ^{3}He with a seven-anode array in a honeycomb pattern. The upper limit of 2θ is 100°. A multilayer [110] silicon wafer monochromator with the reflection from planes of the $<01\overline{1}>$ zone ensures sharp diffraction peaks in specified ranges of detector angles by control of the horizontal radius of curvature.

Any plane from the $<01\overline{1}>$ zone can be set in the Bragg reflection position, but only the (155), (133), (022) with (044), and (111) with (333) reflection planes are of practical interest. For a fixed monochromator angle of 48°, these reflections provide principal incident wavelengths of 0.618 Å, 1.01 Å, 1.56 Å, and 2.55 Å, respectively. A PC-based Lab-View system provides user-friendly

diffractometer control and data acquisition. The beam size is 5×5 mm^2, and the minimum crystal size is 1 mm^3. The maximum crystal dimension is about 4 mm. The flux on the sample is estimated to be greater than 5×10^6 neutron cm^{-2} s^{-1}, whereas that of VIVALDI is 10^9 neutron cm^{-2} s^{-1}.

This instrument is suitable for a wide range of small unit-cell crystallography studies, from structure solution and refinement to charge and nuclear density mapping. Problems have been addressed from chemistry, physics, materials science, and mineralogy. Specific areas of study include hydrogen bonding and weak interactions, organometallics, supra-molecular chemistry and crystal engineering, metal hydrides, charge density, pharmaceuticals, and magnetic structures.

Design for the Future: The ORNL Spallation Neutron Source (SNS) High-Resolution Time-of-Flight Single Crystal Macromolecular Neutron Diffractometer (MaNDi)

The ORNL spallation neutron source is an accelerator-based neutron source and forms a unique facility providing for the most intense pulsed neutron beams in the world dedicated to scientific research and industrial development.

It is reasonable to assume from our previous considerations that neutron macromolecular crystallography (NMC) is capable of providing accurate hydrogen atom positions, protonation states and hydration states, as well as hydrogen/deuterium exchange information in macromolecular crystals. In fact, this is possible even at a moderate resolution of approximately 2 Å. In contrast, in order to observe hydrogen atoms via ultra-high-resolution macromolecular X-ray crystallography, diffraction data beyond 1.0 Å are required. X-ray diffraction beyond this limit can only be achieved with highly ordered crystals, which is rarely achieved. The introduction of the Spallation Neutron Source (SNS) at ORNL with over an order of magnitude increase in neutron flux, in combination with advances in neutron optics and detectors, structural genomics, and protein deuteration, provides new opportunities for NMC to become a routine and essential structural tool for enzymology, structural biology, and functional genomics.

In order to satisfy the needs of the structural biology community, a dedicated, extremely high-quality high-resolution time-of-flight single crystal macromolecular neutron diffractometer (MaNDi) is now under construction at the SNS [15]. The design of this instrument has been optimized so that it will enable data collection rates over 50 times faster than existing facilities. It depends on the high regularity of the neutron pulses from the spallation source and the ability of highly sensitive detectors to distinguish the velocity-dependent wavelength of each particle. This process has been likened to measuring diffraction data from innumerable monochromatic experiments and will enable studies of crystals with lattice constants substantially larger than currently possible. It is expected that the unprecedented speed and resolution limits achievable with MaNDi for NMC experiments will greatly advance the fields of structural biology, enzymology, and computational chemistry.

The SNS macromolecular diffractometer (MaNDi) will be a state of the art high-resolution macromolecular crystal diffractometer. Optimized for rapid data collection from large structures, MaNDi will achieve a 1.5 Å resolution from crystal volumes between 0.1 and 1.0 mm^3 with unit-cell repeats in the order of 150 Å. The instrument will use a decoupled hydrogen moderator for optimal resolution and separation of Bragg peaks. The design utilizes a 24 m flight path and a variable wavelength bandwidth of 2.7 Å to accommodate different types of experiments. This bandwidth variation is achieved by the use of three disc choppers in the incident flight path. With crystals larger than 1 mm^3, it will be possible to obtain useful data in the resolution range 2.0–2.5 Å for unit-cell repeats of up to 300 Å, a revolution in neutron macromolecular crystallography (NMC). Figure 11.5b shows the design of the detector array for the MaNDi instrument.

11.4.3 Other Neutron Sources

We conclude this section with a global list of neutron facilities:
North America
- Spallation Neutron Source, Oak Ridge
- Los Alamos Neutron Science Center (LANSCE)
- University of Missouri Research Reactor Center
- High Flux Isotope Reactor, Oak Ridge
- Canadian Neutron Beam Centre, Chalk River, Canada
- Indiana University Cyclotron Facility

Europe
- ISIS-Rutherford-Appleton Laboratories, UK
- Institut Laue-Langevin, Grenoble, France
- Leon Brillouin Laboratory, Saclay, France
- Berlin Neutron Scattering Center, Germany
- GEMS at Helmholtz-Zentrum Geesthacht, Germany
- Juelich Center for Neutron Science, Germany
- FRM-II, Munich, Germany
- Budapest Neutron Centre, Hungary
- RID, Delft, The Netherlands
- SINQ, Paul Scherrer Institut (PSI), Switzerland
- Frank Laboratory of Neutron Physics, Dubna, Russia
- St. Petersburg Neutron Physics Institute, Gatchina, Russia

Asia and Australia
- ISSP Neutron Scattering Laboratory, Tokai, Japan
- JAEA Research Reactors, Tokai, Japan
- KENS Neutron Scattering Facility, Tsukuba, Japan
- Hi-Flux Advanced Neutron Application Reactor, Korea
- Bragg Institute, ANSTO, Australia

11.5 Deuteration and Perdeuteration

Deuteration
Deuteration even of simple compounds is best effected by collaborating with an experienced chemist. In simple terms, the obvious way to effect H–D interchange would be to soak the compound of interest, or a crystal of it, in D_2O. This may work in some cases, but it is nevertheless a hit-or-miss experiment. Generally speaking, whereas C–H hydrogen atoms would probably not be exchanged in this way, O–H and N–H hydrogen atoms would.

Deuteration may be carried out on pre-grown crystals or on the pure sample itself prior to crystallization. With some crystal materials that are sensitive to liquids, it may not be possible to perform the experiments necessary to effect deuteration, Sect. 11.7; help can be obtained from appropriate websites [16–18].

Perdeuteration or Biodeuteration
Neutron protein crystallography provides a powerful complement to X-ray crystallography by enabling key hydrogen atoms to be located in biological structures where they cannot be seen by X-ray analysis alone. The neutron Laue diffractometer LADI, run jointly by EMBL and ILL at the

ILL high flux reactor in Grenoble, is a dedicated facility for neutron protein crystallography at high-resolution (1.5 Å) and provides 10–100-fold gains in efficiency compared with conventional neutron diffractometers. The availability of a fully deuterated (perdeuterated or biodeuterated) protein eliminates the hydrogen incoherent scattering contribution to the background and brings approximately tenfold improvements in the signal to noise ratios.

The production of deuterium-labeled macromolecules is carried out using bacterial expression systems incorporating perdeuterated glycerol $(CH_2OH)_2CHOH$ as the sole carbon source in the Deuteration Laboratory at Grenoble [19]. Protein crystals are grown using methods described in Chap. 10, but with D_2O replacing H_2O. A recent paper [20] provides an up to date example of this type of research.

The aim of the facility at the Institut Laue-Langevin, in collaboration with the European Molecular Biology Laboratory, is to provide a focus for scientists wishing to make their own deuterated materials prior to carrying out neutron scattering experiments. In support of the effort to encourage deuteration studies, a major EU grant has been obtained jointly by ILL, EMBL, the University of Oxford, and the Institut de Biologie Structurale, Grenoble in order to develop different protocols and procedures of deuteration both for neutron scattering and NMR studies.

11.6 Examples of Structure Determination by Neutron Crystallography

We now discuss in detail three recent examples of single-crystal analyses that have been enhanced through the use of neutron diffraction. The first example is an atomic resolution study of a small organic molecule, the second is an intermediate resolution study of a lectin protein molecule, and the third is a high-resolution analysis of the 11-membered peptide cyclosporin H. All three examples combine, for reasons given previously, the neutron study with a parallel X-ray study, and they illustrate different aspects of the current state of neutron diffraction technology, indicating its versatility and potential. We show during the determination of the first structure how potential pitfalls of "black box" crystallography can be encountered.

11.7 X-Ray and Neutron Structure of 1,8-(3,6,9-Trioxaundecane-1, 11-diyldioxy)-9,10-dihydro-10-10 dimethylanthracene-9-ol [21]

This compound was prepared in high yield by bis-methylation of anthralin at the 10-position, followed by bis-*O*-alkylation to give a ketone (I) that was reduced to the alcohol by sodium amalgam. A detailed molecular structure of the formal hydrolysis product, Fig. 11.6, of the parent cationic form, Fig. 11.7, was required.

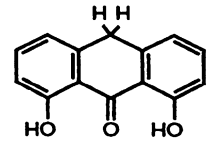

I

The product has been shown from combined X-ray and neutron diffraction analyses to be 1,8-(3,6, 9-trioxaundecane-1,11-diyldioxy)-9,10-dihydro-10,10-dimethylanthracene-9-ol, and is the parent compound for an important series of derivatives; unequivocal positions for the hydrogen atoms were obtained from this study. Both sets of data were measured on single crystal four-circle diffractometers with monochromatic radiation. In terms of the X-ray analysis, there were 96 carbon

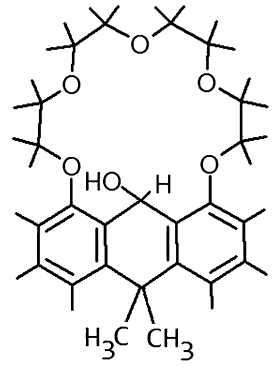

Fig. 11.6 The molecular structure of 1,8-(3,6,9-trioxaundecane-1,11-diyldioxy)-9,10-dihydro-10,10-dimethylanthracene-9-ol

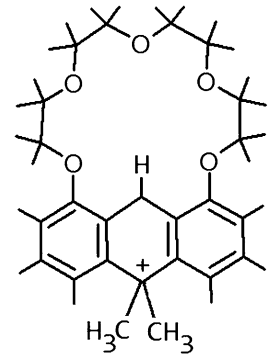

Fig. 11.7 The cationic form of the compound illustrated by Fig. 11.6

atoms and 28 oxygen atoms per unit cell. A solution of this structure by direct methods was therefore quite feasible. In the neutron structure diffraction analysis, a further 128 hydrogen atoms of comparable size (in neutron diffraction terms) to the carbon and oxygen atoms were present per unit cell. Solution of the neutron structure ab initio was therefore not attempted; it was solved by a Fourier expansion of the X-ray structure. This process was not impaired by the changes in unit cell related to the different experimental temperatures used in the two analyses. The crystal and structure analyses data for this compound are summarized in Table 11.2.

11.7.1 Experimental

Sample Preparation

The slow evaporation of an ethanolic solution yielded crystals of melting point 151–153°C, which were used in the crystallographic studies. No attempt was made to exclude water from the purified solvent used for crystallization. However, the presence of water in the crystalline material was not evident from its spectra.

Table 11.2 X-ray and neutron crystal data for 1,8-(3,6,9-Trioxaundecane-11-diyldioxy)-9,10-dihydro-10,10,10-dimethylanthracene-9-ol

Chemical formula	$C_{24}H_{30}O_6 \cdot H_2O$	
M_r	432.50	
Color/shape	Colorless/plates	
	X-ray	*Neutron*
Temperature	293(2) K	15 K
Crystal system/space group	Monoclinic/$P2_1$	Monoclinic/$P2_1$
Unit cell dimensions/Å (25 reflections with $25 < \theta < 30°$)	a 12.845(5) b 14.575(3) c 13.779(2) β 117.72(2)°	12.605(5) 14.458(3) 13.588(2) 117.12(2)°
Unit cell volume/Å^3	V_c 2283.6(1)	2204.1(1)
Z (2 molecules/asymmetric unit)	4	4
D_c (g cm^{-3})	1.258	1.302
μ_c (cm^{-1})	0.754	0.754
Diffractometer/scan	Nonius CAD4/$\omega-2\theta$	D19 ILL/ω
Radiation	Cu $K\alpha$	Neutron
Monochromator	Graphite	Graphite
Wavelength (Å)	1.54180	1.538, 1.312
Crystal dimensions (mm)	0.35, 0.25, 0.20	2.5, 1.6, 0.2
Reflections measured	17753	1931
Independent/observed	9092/9092	1931/1881
R_{int}	0.0459	
$\theta_{max°}$	72.93	46.12
Range of *h, k, l*	$\mp 15, \mp 18, \mp 17$	$\overline{10}-11, 0-13, \bar{9}-12$
Data processing	CAD4-Express 1992	RETREAT
Structure solution	SHELX-S-86	From X-ray
Structure refinement	SHELXL-97	SHELXL-97
Refinement method	Full-matrix least-squares on F^2	
Data/restraints/parameters	9092/217/605	1881/1/507
Goodness-of-fit on F^2	0.908	0.779
Final R [$I > 2\sigma(I)$] R_1/wR_2	0.0619/0.1506	0.0462/0.1184
R indices (all data) R_1/wR_2	0.1001/0.1688	0.04093/0.1320
Absolute structure parameter	0.25(35)	
Largest diff. peak/hole	0.232/-0.260	0.055/−0.058

X-Ray Diffraction Measurements

A crystal was centered on a Nonius CAD4 diffractometer. The software package CAD4 Express 1988 was used to determine a unit cell and orientation matrix based on 25 reflections selected by the software, employing Cu $K\alpha$ radiation. The diffractometer system, in automatic mode, favored an orthorhombic *C*-centered cell which refined to the dimensions listed in Table 11.2.

The assignment of crystal system by the software was based solely on the close proximity of the cell angles to 90°. This software was designed to collect one asymmetric unit of intensity data for the initially assigned point group, there being no automatic Laue check facility at this stage. However, it was possible to carry out a check for Laue symmetry after data collection, but this was not an easy procedure to carry out with this version of the software. We note that the later version of the software

(CAD4 Express, 1994) does carry out a Laue check in automatic mode prior to data collection proper. Intensity data were routinely collected for one asymmetric unit of assumed orthorhombic reciprocal space, for $1 < \theta < 74°$.

The space group was assigned by inspection of the systematic absences in the intensity data, after processing in $C222_1$. The unit cell was calculated to include eight molecules of $C_{24}H_{30}O_6$ (two molecules per asymmetric unit). It was discovered subsequently, during refinement of the structure, that there were additionally two water molecules per asymmetric unit. It should be noted that the X-ray results were obtained under some pressure, being required urgently in order to coordinate with a scheduled neutron data collection time at ILL. Therefore, the X-ray analysis proceeded at this stage without any hint that an extraordinary situation would soon arise as a result of a very unusual geometrical relationship between the unit-cell parameters. These parameters appeared to be quite reasonable at this stage of the analysis. The crystal had moderate diffracting power and good single-crystal quality was indicated from the diffractometer readings incorporated into the software. The first X-ray data set, after processing and correction for Lorentz and polarization effects, gave 2572 unique intensities, 1395 with $F_o > 4\sigma(F_o)$, and with few symmetry repeats R_{int} was indeterminate.

The direct methods program SHELX-S produced no solution in space group $C222_1$. The monoclinic space group $C2_1$ was then tried (non-standard, c-unique setting: determine what this is equivalent to and draw a space-group diagram). It produced an outstanding solution giving a promising E map which contained the essential features of both molecules in the unit cell, despite being based on only part of the monoclinic data set, through an incorrect assumption of the point group. This structure failed to refine properly, owing to the incompleteness of the "orthorhombic" intensity data set. The best R-factor achieved with this model using isotropic thermal displacement parameters was 0.24, with a data/parameter ratio of 10.8.

A second set of intensity data was collected, with the unit cell constrained to be monoclinic, an option allowed by the software. The data for the monoclinic unit-cell and other data are listed in Table 11.2. A total of 9092 unique, corrected (excluding absorption) intensities was recorded, 4804 with $F_o > 4\sigma(F_o)$, with $R_{int} = 4.59\%$. Subsequent refinement of the X-ray structure, Sect. 11.7.2, confirmed this assignment of unit cell and space group.

Neutron Diffraction Measurements

Prior to the start of the neutron diffraction data collection, the reflection indices and cell parameters of the octant of X-ray diffraction data that had been collected in the monoclinic C-centered setting were transformed to a primitive, monoclinic setting with b-axis unique and space group $P2_1$. A crystal with approximate dimensions 2.5, 1.6, 0.2 mm was mounted on a vanadium support on the D19 four-circle diffractometer at ILL, with the longest unit-cell dimension of the plate along the diffractometer ϕ-axis. The neutron wavelength was 1.538 Å and an initial scan of reciprocal space located six reflections which could be indexed and a preliminary orientation matrix calculated. Additional reflections, which were expected to be of significant intensity on the basis of the X-ray data, were then located and an improved orientation matrix established.

The $4 \times 64°$ area detector of D19 enabled the three-dimensional peak shapes of the Bragg reflections to be monitored, and neither splitting nor streaking was observed. The crystal was cooled to 15 K while a strong reflection was continuously monitored and a new orientation matrix established. The peak shapes of a number of reflections were checked. Collection of the $\pm h\bar{k}\,\bar{l}$ data commenced in shells of $2\theta = 92°$, using ω-scans in equatorial geometry. The area detector allowed additional reflections to be measured and so checks were made of mirror-related reflections and repeated measurements of the same or Friedel-related (q.v.) reflections, as well as the usual three reference reflections repeated regularly during data collection.The wavelength was then changed to 1.312 Å in order to measure higher-angle data, a new orientation matrix calculated and data collection

continued using normal beam geometry. Because of a slow helium leak, a significant reduction in detector efficiency had occurred. Nevertheless, the efficiency was effectively constant on the time scale of the experiment, but this situation, and the rather small crystal volume of 0.8 mm^3, contributed to the fact that half of the intensity data were weak, although significantly above background. The program RETREAT was used to integrate the Bragg peaks in three dimensions. No absorption correction was applied, although the crystal shape would have caused certain reflections to have suffered significant absorption effects. The data were merged and sorted to provide 1931 unique reflections.

11.7.2 Structure Analysis and Refinement

X-ray Structure

Using the monoclinic X-ray data set, the direct methods routine in SHELX-S produced an outstanding solution to the structure in space group $P2_1$. The corresponding E map revealed the positions of all non-hydrogen atoms in both molecules (here designated A and B). Difference electron density maps indicated the presence of bound water in each molecule. The structure was completed and refined by full-matrix least-squares on $|F|^2$, with anisotropic displacement parameters for non-hydrogen atoms, and isotropic parameters for the hydrogen atoms, which were fixed geometrically in riding mode. Methyl group hydrogen atoms were located using the circular Fourier facility in SHELXL-93; only one hydrogen atom was found on each water molecule in the difference electron density maps.

The structure refined to convergence with SHELX-97 with a mean σ/err of 0.020 (max. 0.071); soft constraints (SADI) were applied in order to equilibrate bond distances between molecules A and B. The final measures of agreement for a total of 9092 reflections with $I > 2\sigma(I)$ and 605 parameters are listed in Table 11.2 together with those for the neutron analysis which follows.

Neutron Structure

At the start of the refinement, the coordinates from the X-ray refinement were used together with the F_o data from neutron diffraction. Unexpectedly there was no agreement, although the unit-cell parameters from the two sets of measurements were in close agreement, and any difference could be ascribed to the temperature difference between the two sets of measurement conditions. This situation, which gave considerable cause for concern, was traced eventually to the idiosyncrasies in the shape of the unit cell. Thus, when the transformation from the original X-ray, apparently rectangular, *C*-centered cell to the correct, primitive monoclinic cell was made, two alternative but extremely similar unit cells could be chosen as shown in Fig. 11.8. It transpired that, by chance, one unit cell had been chosen for the X-ray data collection and the other for the neutron data. The two intensity data sets were therefore not matched. In order to rectify this situation, the indices and cell parameters of the neutron data were suitably transformed and the analysis was then carried out as described below.

The β-angle now established differs from that listed in Table 11.2 because the γ-angle was inadvertently and incorrectly assumed to be exactly 90° instead of the true value of 90.10°.

The atomic coordinates from the X-ray refinement, which were now compatible with the transformed unit cell and *hkl* neutron data (at $R = 0.10$), were used as the starting set for the neutron structure. Isotropic refinement led rapidly to an *R*-factor of 0.06. Although the X-ray structure had revealed most of the hydrogen atoms, one hydrogen atom from each water molecule had been undetected. A difference neutron synthesis revealed the missing atoms. Refinement was undertaken by

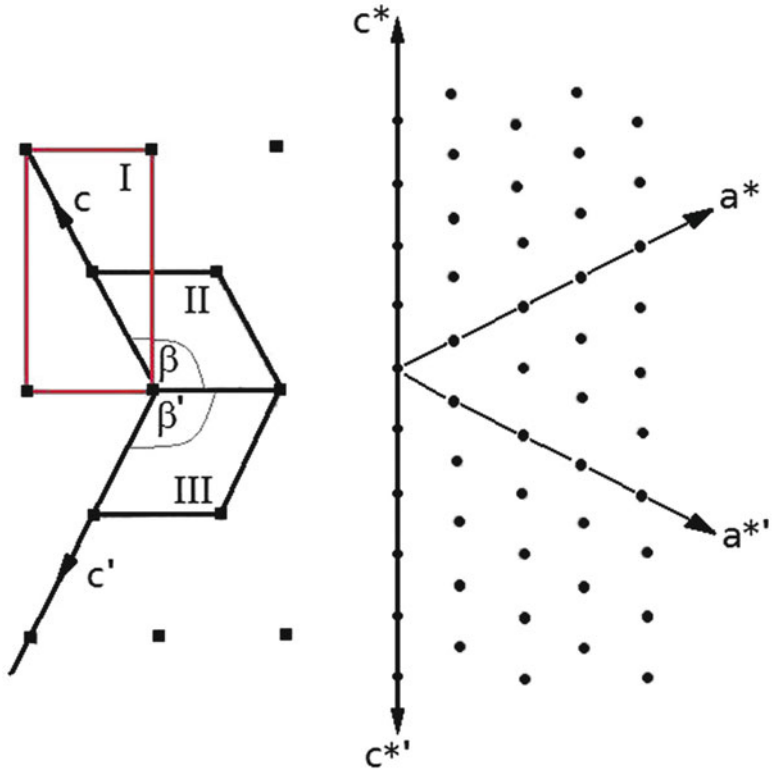

Fig. 11.8 Relationship between alternative unit-cell transformations. (**a**) Crystal unit cells. (**b**) Reciprocal lattice. Note that I is the *ab* face corresponding to the original *C*-centred X-ray unit cell. The angle γ of this unit cell is not exactly 90 but $=90.1(1)^\circ$ and consequently the derived primitive true monoclinic cells II (the transformed X-ray cell) and III (the original neutron cell) have slightly different β angles of 117.93(2) and $=117.12(2)^\circ$, respectively. Only the values of unit-cell parameters c and β are changed by this modification, and the indices transform as $h' = h$, $k' = -k$, $l' = -(l + h)$

full-matrix least-squares on $|F|^2$, with isotropic displacement parameters for all atoms. The structure was refined to convergence using SHELX-97. The final measures of agreement are listed in Table 11.2. The least-squares refinement converged with a mean σ/err of 0.006 (max. −0.12). Neutron scattering lengths were taken from Volume III of the International Tables for X-ray Crystallography (1952).

11.7.3 Discussion of the Structure

The unit cell dimensions for the "orthorhombic" unit cell, suggested by the version of the software for the CAD4 then available, were $a = 12.856(1)$ Å, $b = 24.396(4)$ Å, $c = 14.564(2)$ Å, $\alpha = 89.98(1)^\circ$, $\beta = 89.987(9)^\circ$, $\gamma = 90.10(1)^\circ$. The potential for designing automated diffractometer systems without adequate symmetry checks and the dangers of misuse with some automated diffractometer systems became clear. We emphasize strongly the importance of the role of photographic methods, which are still in use in many laboratories and teaching schools, and/or an early Laue photograph to check the determination of the Laue group and crystal system. We believe that many important

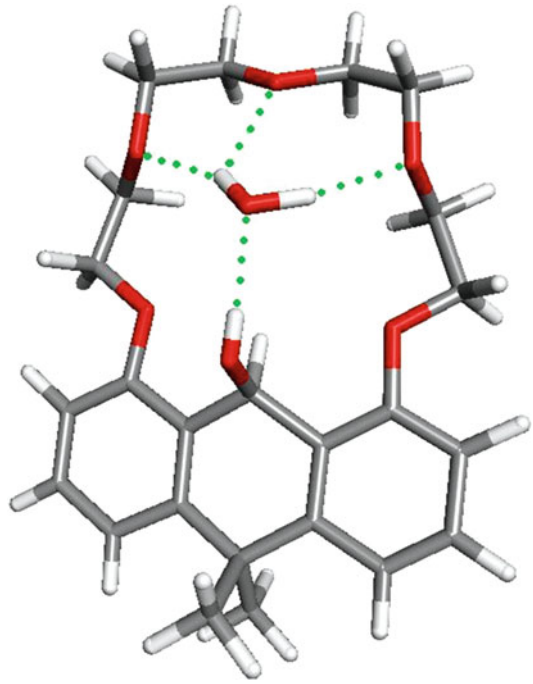

Fig. 11.9 Molecule A from the neutron diffraction analysis, showing the water molecule and the hydrogen bonding (built by Accelerys)

structures may be passed over or discarded through a failure to use, or simply a lack of awareness, of these procedures. The other crystallographic situation illustrated by this structure is the possibility of different unit-cell choices appearing identical, with the consequential difficulties in the comparison of structural data.

11.7.4 Hydrogen Bonding

The hydrogen bonding was elucidated from the neutron diffraction results. Molecules A and B exhibit similar hydrogen bonding patterns, there being strong interactions between each molecule and its solvated water, Figs. 11.9 and 11.10. There are no hydrogen bonds between the molecules A and B, or otherwise.

Each molecule includes a hydrogen-bonded water molecule which stabilizes the macrocyclic ring structure. Both molecules A and B exhibit very close pseudo-symmetry across a plane perpendicular to the molecular plane and through atoms C(9) and O(18); in addition they show predominantly planar structures. The crystal packing includes hydrogen bonding patterns for molecules A and B, with three strong interactions between each molecule and its solvated water. The X-ray analysis failed to reveal one hydrogen atom per water molecule, each being subsequently included after location and refinement in the neutron analysis. The initial automatic assignment of a very convincing "orthorhombic" X-ray unit cell and the subsequent monoclinic transformations in the two analyses reaffirms the need for caution in applying procedures automatically.

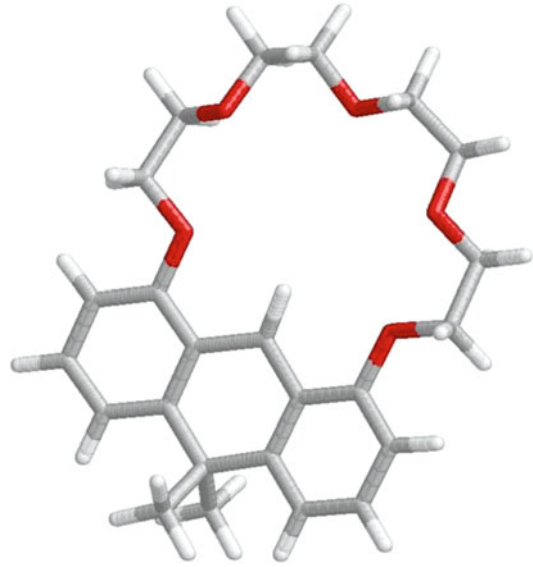

Fig. 11.10 The structure of molecule B, built from molecule A using Accelerys and drawn with RASMOL

11.8 The Pointless Program in CCP4

We conclude this section on a slightly more optimistic note. It has been drawn to our attention that since the above research was undertaken a new CCP4 program known as Pointless [22] has become available. Using the observed $F_o(hkl)$ data, this program determines all the possible Laue groups consistent with the unit cell, which is based on cell dimension restraints. It does this by matching potential symmetry equivalent reflections. For chiral systems, the Laue group uniquely implies the point group. It then checks sets of reflections which may be systematically absent to suggest a possible space group. There is no check for unit-cell centering, that is, no check for whole classes of reflections having zero intensity, although there is a check for potentially centered reflections missing from the list. Strictly speaking, the program determines the "Patterson group" rather than the Laue group, since the Laue group is a point group, but not combined with any unit-cell centring type (P, C, I, F, H, or R). Unit-cell centring is included in the reported Laue group, and re-indexing from the original setting may change the unit-cell type.

11.9 Determination of the Positions of the Deuterium Atoms of the Bound Water Molecules in the Lectin Protein Concanavalin A by Neutron Laue Crystallography [23]

11.9.1 Introduction

Concanavalin A is a saccharide binding protein isolated from the Jack Bean and is the most thoroughly studied member of a class of proteins known as plant hemagglutinins or lectins [24]. Its biological role is unknown, but it is thought to mediate cell–cell interactions by binding to polysaccharide on the cell surface. It may also have an antifungal plant-defense role. The molecule has a

molecular weight of 25 kDa, contains 237 amino acids, and binds a calcium and a transition metal ion, for example Mn, as in the present structure.

Structural studies by neutron diffraction permit elucidation of hydrogen/deuterium exchange, which can yield vital information for the understanding of catalytic processes at the molecular level [25]. This approach exploits the difference in neutron scattering lengths between hydrogen and deuterium, which are equal under X-ray diffraction. Hydrogen atoms constitute a large proportion of any biological material and to understand the structure or the catalytic mechanism of such materials it is desirable to locate those atoms. Exchanging hydrogen for deuterium in a neutron diffraction experiment has three advantages:

1. A possible reduction of the incoherent scattering by hydrogen.
2. Deuterium has a neutron scattering length of 6.671, which is similar in sign and magnitude to those of the other atoms of the protein, whereas hydrogen has a scattering length of −3.739; this allows contrast-variation studies.
3. Deuteration also improves the determination of water deuterium atom positions, as the scattering lengths of deuterium and oxygen are both positive in sign and the shape of the D_2O nuclear density indicates the D_2O orientation.

A high level of D_2O exchange is important in a detailed study of bound water by neutron diffraction. In addition to the bulk water and water of hydration, which comprise approximately 50% of most protein crystals, the exchangeable atoms are those attached to nitrogen or oxygen atoms, namely:

1. Main chain N–-H bonds (except in prolines).
2. The side chains of Thr, Tyr, Asn, Ser, His, Lys, Arg, Trp, and Gln with N–H or O–H bonds.
3. The side chains of Asp and Glu, if originally protonated.

The unexchangeable hydrogen atoms in the structure are those attached to carbon atoms, as in C–H bonds, for example. In concanavalin A, there are 399 exchangeable hydrogen atoms and 1356 that are non-exchangeable.

11.9.2 Deuteration of the Concanavalin A Crystals

Large crystals of concanavalin A were selected for the neutron study. They were transferred to a 1 ml portion of crystallization buffer in a tightly sealed test tube. The D_2O solution was changed four times during the four-month soaking period. The crystal form studied here has the space group *I*222. The chosen crystal, of dimensions 3, 2.5, 2 mm, was mounted in a quartz capillary and used for neutron diffraction data collection on the LADI diffractometer at ILL, as discussed above.

11.9.3 Data Collection and Analysis

In the data collection, the range of neutron energies corresponding to a wavelength range of 2.49–3.52 Å was obtained using a system of silicon crystal mirrors each with 748 alternating 74–90 Å thick titanium and nickel layers. The shift towards shorter wavelength helps to enhance the resolution of the data. A total of 20 neutron Laue images were collected from −60 to +54° in intervals of 6°. The exposure time per image was 23.5 h; 5 min were needed to scan and download the data from the image plate and one minute to erase it before re-use.

The neutron Laue data were processed using the Daresbury Laboratory software developed for synchrotron Laue data processing, but modified for neutron Laue data with a cylindrical detector geometry of diameter 318.3 mm. The orientation of the crystal was determined by automatic indexing

Table 11.3 Bound neutron coherent scattering lengths

Atom type	Scattering length (fm)
H	−3.74
D	6.67
C	6.65
N	9.36
Ca	4.70
Mn	−3.73

of the spots using the LAUEGEN program, as was the prediction of the spots of each image. The unit cell was refined by LAUEGEN and the unit-cell parameters determined were $a = 88.7$ Å, $b = 86.5$ Å, and $c = 62.5$ Å. The resolution limit was 2.4 Å. The INTLAUE program was used for integration of each Laue reflection, and the LAUENORM program was used to derive the wavelength-normalization curve using the intensities of symmetry equivalent reflections measured at different wavelengths. This essentially puts all of the reflections on the same wavelength basis. A unique set of 8605 reflections from these measurements was produced giving a final working neutron data at 2.4 Å resolution.

The neutron Laue geometry employs a much broader band of neutron wavelengths than a monochromatic beam and, with a very large image-plate detector, allows data collection in a reasonable time, days instead of months, for small crystals and structures with large unit cells.

11.9.4 X-Ray Model Refinement

In order to carry out a neutron diffraction refinement of the concanavalin A structure, a good quality starting model at an appropriate resolution was first needed, and to this end an X-ray data set was measured using a crystal of dimensions 1.6, 0.95, 0.5 mm deuterated under the same conditions as the crystal used for the neutron diffraction measurements. The X-ray data set was collected using an R-AXIS II area detector with Cu $K\alpha$ (rotating anode) radiation. The data were processed in DENZO/SCALEPACK. The refined unit-cell parameters were $a = 89.11$ Å, $b = 87.58$ Å, and $c = 63.26$ Å. There were 24110 unique reflections to a resolution of 1.7 Å. The X-ray structure was generated with respect to this data set using as a starting model the coordinates from the PDB file [26] and refined using X-PLOR to 1.8 Å resolution. In this X-ray model, hydrogen (deuterium) atoms were generated for the bound water oxygen atoms using X-PLOR.

11.9.5 Neutron Structure Refinement

The refined X-ray structure of the deuterated crystal at a resolution of 1.8 Å, determined as described in the previous section, was used as the starting model for the neutron refinement using X-PLOR version 3.851. The structure, including the calculated hydrogen atoms, comprised 3566 protein atoms and 148 water molecules. The neutron scattering lengths used throughout all the subsequent refinements were those of the Atomic Energy of Canada (1992) as shown in Table 11.1 and 11.3.

The unit cell used was determined during the course of the Cu $K\alpha$ X-ray data reduction. Using LSQKAB [27], the two models were superimposed and the average displacements for the 444 bound water molecules calculated to be 0.04 Å. For water molecule six, featured in Fig. 11.11, the oxygen atom shift was 0.03 Å. The interpretation of hydrogen/deuterium exchange in the peptide chain was also needed and, in order to undertake this, the output model of the final cycle of X-PLOR neutron

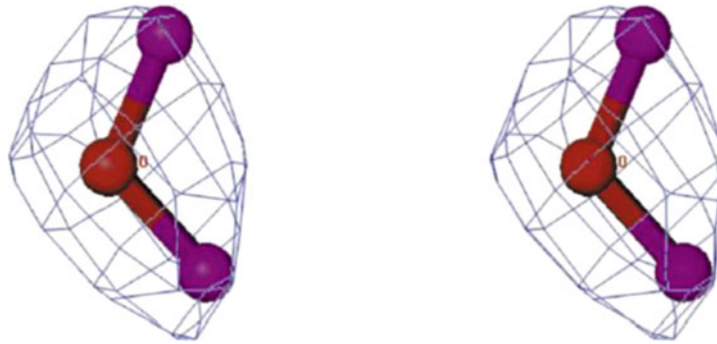

Fig. 11.11 Stereo diagram showing the orientation of a well-ordered molecule of D_2O, number 6 in the PDB, in the neutron density

refinement was input to SHELXL to determine the occupancy refinement. To determine the extent of hydrogen/deuterium exchange of the N–DH amides on the protein (228 atoms), the occupancy of each exchangeable hydrogen atom was tied to the occupancy of a deuterium atom so that the sum of their occupancies was constrained to be equal to 1.0. The occupancies of hydrogen and deuterium varied from 0 to 1.0 for most of the peptides.

11.9.6 The Bound Water Structure

There are 148 bound water molecules to be investigated. Many water molecules appear as D_2O with elongated positive density. The water deuterium atoms are thereby important contributors to the overall scattering. There are many examples where the initial hydrogen atom positions assigned by X-PLOR to the X-ray model were not found in the nuclear density map, but after refinement against the neutron data the fit to the density was greatly improved and taken to be correct. These are water molecules that are hydrogen-bond donors or acceptors either with the protein or with other water molecules, for example, in water clusters. Figure 11.11 is a stereo illustration of a well-ordered D_2O molecule where the oxygen atom and its two deuterium atoms enhance one another so to give a positive neutron density with a shape evident for the nuclear density. Two water molecules, numbered 22 and 27 in the PDB file 1c57, which may be downloaded from the Protein Data Bank, are coordinated to the Mn atom in the transition metal-binding site, and another two water molecules, numbers 29 and 30, are coordinated to the Ca atom in the nearby calcium-binding site. They are illustrated in Figs. 11.12, 11.13, and 11.14. Of the 148 defined bound waters, 93 are in the primary hydration shell and 55 are in the secondary hydration shell.

11.9.7 The Metal Sites

The transition metal manganese is coordinated to Glu8, Asp10, Asp19, His24, and two D_2O water molecules. The neutron scattering length for manganese is -0.373, essentially the same as the scattering length of hydrogen, and is observable in the negative density. The distances of Mn and Ca from their ligands as determined in this study by the X-ray refinement are shown in Tables 11.4 and 11.5, respectively.

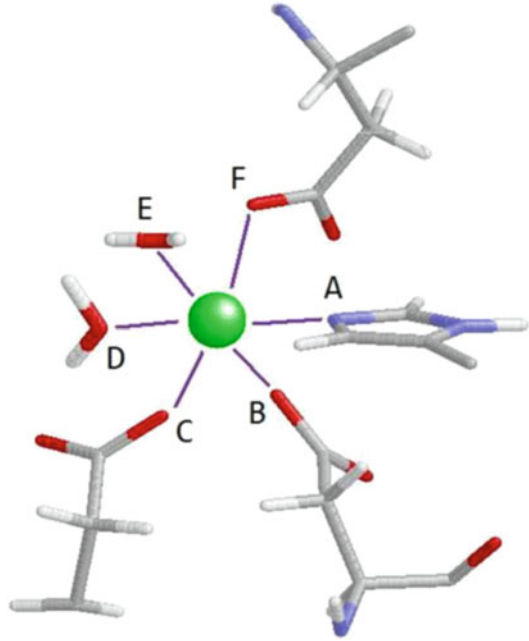

Fig. 11.12 Mn coordination sphere, Table 11.4, drawn with RASMOL; see also Problem 11.5

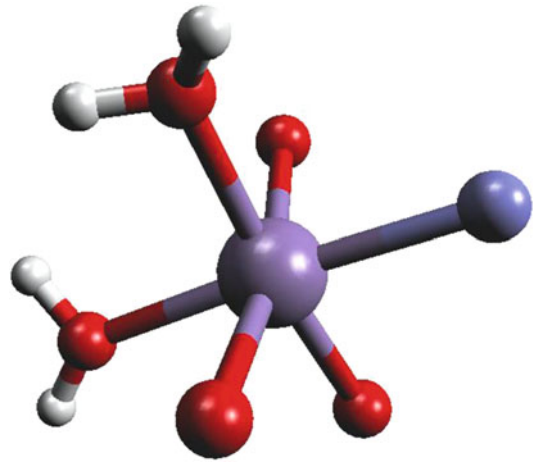

Fig. 11.13 The Mn coordination *sphere*

11.9.8 The Saccharide Binding Site

In the saccharide-free crystal form studied here, the saccharide binding site is occupied by the three water molecules 31, 34, and 33, which form hydrogen bonds to the protein as shown in Figs. 11.15 and 11.16.

Water molecule 31 is hydrogen bonded to both water molecules 33 and 34. It is probable that water molecule 33 is hydrogen bonded to water molecule 34, and thus the three water molecules are linked to form a triangle. These water molecules fill the binding site snugly and water molecules 33 and 34 form hydrogen bonds to the adjacent protein. Water molecule 33 donates deuterium to form a

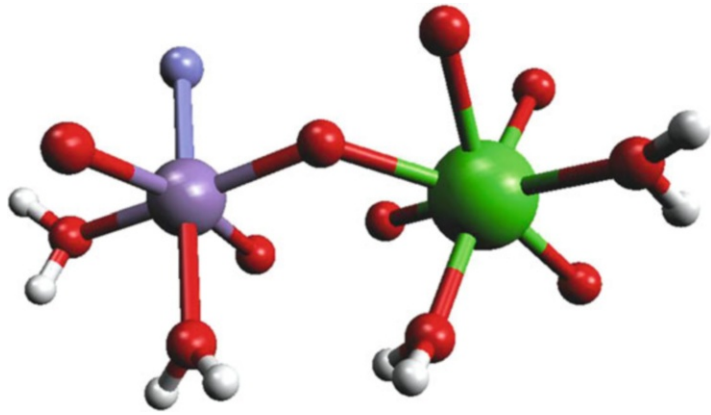

Fig. 11.14 The Mn and Ca coordination spheres; note the common link from OD1 (Asp 10)

Table 11.4 The Mn coordination-sphere ligands

Mn–Ligand	Distance (Å)
Mn-OE1 (Glu8)	2.19
Mn-OD1 (Asp10)	2.17
Mn-OD1 (Asp19)	2.24
Mn-NE2 (His24)	2.28
Mn-O (water 22)	2.17
Mn-O (water 27)	2.28

Table 11.5 The Ca coordination-sphere ligands

Ca–Ligand	Distance (Å)
Ca-OD1 (Asp10)	2.47
Ca-OD2 (Asp10)	2.48
Ca-O (Tyr12)	2.34
Ca-OD1 (Asn14)	2.36
Ca-OD2 (Asp19)	2.44
Ca-O (water 29)	2.42
Ca-O (water 30)	2.38

hydrogen bond to Asp208 OD1, while its oxygen atom can form a hydrogen bond to the adjacent Asn14 HD22. Water molecule 34 is close enough to form hydrogen bonds to Tyr100 HN and Asp208 OD2.

11.9.9 Conclusion

This neutron diffraction study has provided details of the manganese ligand environment, that is, the coordination of the hydrogen and deuterium atoms of the two associated water molecules that are necessary for an in-depth understanding of features such as the EPR spectroscopy of Concanavalin A. The extensive direct soaking of the crystal in D_2O has yielded the deuterium atom

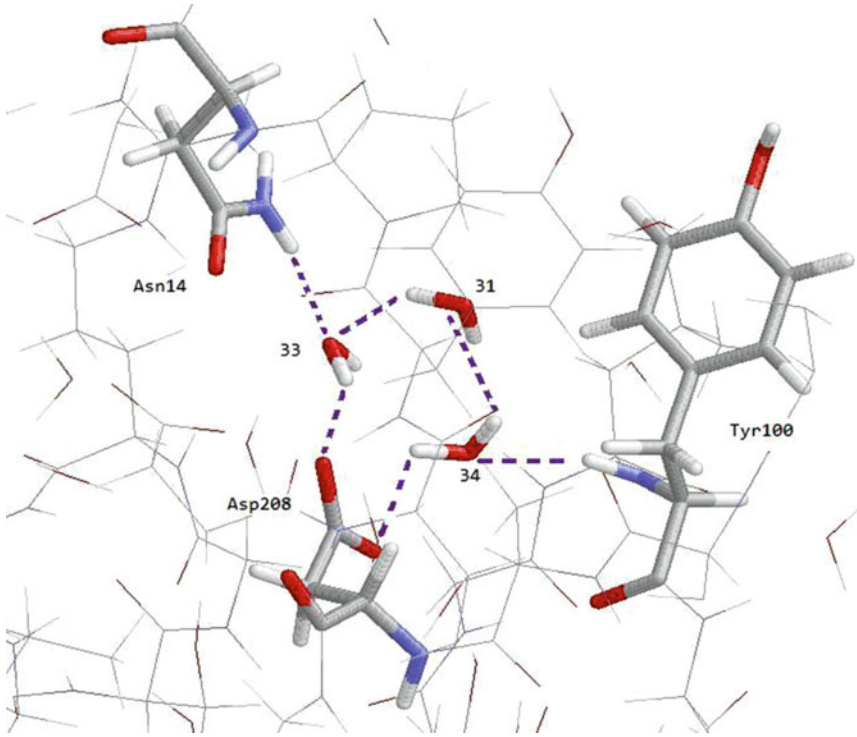

Fig. 11.15 The saccharide binding site, drawn by RASMOL

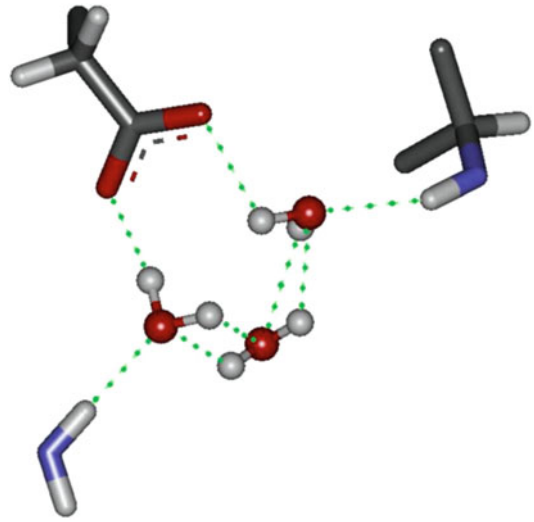

Fig. 11.16 Saccharide binding site details, built by Accelerys

positions of the bound water molecules. The reduction of the number of hydrogen atoms via this D_2O soaking method has also enhanced the neutron diffraction resolution.

Neutron diffraction of the bound D_2O molecules, even at the relatively low resolution of this study, is seen to be more effective than ultra-high-resolution X-ray diffraction, assigning many more

coordinates of the deuterium atoms in bound D_2O; 62 complete D_2O molecules were revealed, plus 20 with only one deuterium atom, as well as oxygen. In comparison, for the bound water in the ultra-high-resolution X-ray structure, there are only twelve complete H_2O molecules, plus 35 with one hydrogen atom visible, as well as oxygen, and 272 with no hydrogen atom visible even at 110 K. Thus, the complementarity of the neutron and X-ray approaches is clearly evident.

In the saccharide binding site of concanavalin A, the neutron study has revealed the deuterium atoms of the bound water molecules at that binding site. As a sugar ligand approaches the receptor binding site on the protein, the mutual orientation of these water molecules together is now known. This is a new level of detail for molecular recognition and molecular modeling studies in the future.

Joint X-Ray and Neutron Refinement

It may be noted that it is possible to combine X-ray diffraction data with neutron diffraction data and to carry out refinement using both sets of data simultaneously. In this way the data-parameter ratio can be substantially increased, thus effecting significant improvements in the refined model. This has been undertaken most extensively on protein structures [28]. The best results are obtained if the same crystal can be used in the measurement of both sets of data, or if this is not possible to use two crystals grown in the same crystallization experiment. This ensures that the two crystals are isomorphous.

11.10 The Neutron Structure of the Formyl Peptide Receptor Antagonist Cyclosporin H (CsH) Unambiguously Determines the Solvent and Hydrogen Bonding Structure for Crystal Form II [16]

11.10.1 Introduction

In the final example of these three recent neutron diffraction studies, we describe the analysis carried out on Cyclosporin H in order to resolve some minor problems that were encountered in an earlier X-ray study: we do not report that study [29] here, but use the X-ray coordinates from it in this neutron structure determination. Single-crystal neutron diffraction data have been collected at 20 K to a resolution of 1.05 Å on a crystal of the inverse formyl peptide receptor agonist Cyclosporin H (CsH-II) on the VIVALDI Laue diffractometer at ILL, Grenoble. The solvent structure and hydrogen bonding network of CsH-II have been unambiguously determined by single-crystal neutron diffraction; the agreement factor on $|F|^2$ is 13.5% for all 2726 reflections. All hydrogen atom positions, including methyl group orientations, have been determined by crystallographic refinement. The neutron diffraction structure of cyclosporin H provides unique and complementary insights into methyl orientation, hydrogen bonding, and solvent interactions that are not available from X-ray analysis alone.

The hydrogen atoms in a biological material play an essential part in its structure and function. For a full understanding of hydrogen bonding and solvent structure, it is essential to know the accurate locations of the hydrogen atoms in various situations: terminal $–CH_3$, –OH groups, and solvated water molecules. Neutron diffraction enhances the possibility of determining their locations reliably. Cyclosporins are cyclic undecapeptides of fungal origin, the best known of which, cyclosporin A (CsA), is a lead clinical immunosuppressant; cyclosporin H is an inverse formyl peptide receptor agonist, differing from CsA only in the chiral inversion of MeVal-11 from L to D configuration. The peptide sequence of cyclosporin H is (L)Bmt-(L)Abu-Sar-(L)MeLeu-(L)Val-(L)MeLeu-(L)Ala-(D)Ala-(L)MeLeu-(L)MeLeu-(D)MeVal. The X-ray structure of CsA crystallized from chloroform shows a very similar conformation to that determined by both ^1H and ^{13}C NMR spectroscopy in chloroform solution. Several other crystal forms of CsA and derivatives, crystallized from a range of solvents, including ethanol, ether, and acetone, have also been examined; in most cases the CsA

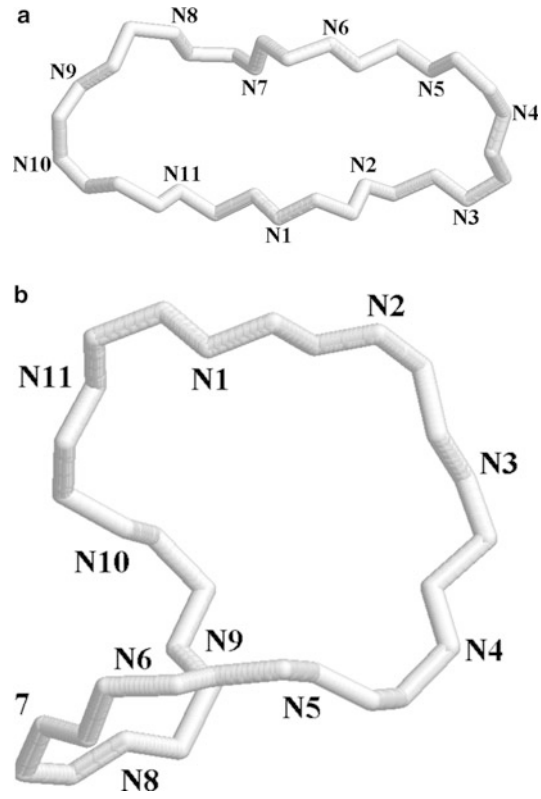

Fig. 11.17 A single stereochemical inversion at residue 11 induces the conversion of Cyclosporin A (**a**) to cyclosporin H (**b**); the structures adopt dramatically different loop configurations. The peptide nitrogen atoms are labeled. CsA data was taken from PDB 2WFJ, and the figures drawn with RASMOL

conformation is very similar to within about 0.2 Å for α-carbon atoms. These studies include crystallographic (X-ray and neutron) and NMR spectroscopic studies of CsA and its complex with cyclophilin.

Two detailed X-ray crystal structure determinations of CsH [30], crystallized in the presence or in the absence of Mg^{2+} (forms I and II, respectively), have been undertaken at 0.80 Å resolution and have identified structural and surface features important for biological activity which may aid the future design of new CsH derivatives. A major and surprising outcome of this X-ray study was the observation that a *minor* local chemical change between CsA and CsH— the chiral inversion of one peptide—is associated with a *major* structural transformation from open β-sheet in CsA to a saddle-shaped "baseball-stitch" conformation in CsH, Fig. 11.17a, b.

CsH forms I and II both adopt the same saddle-shaped secondary structure, and the peptide bonds in this highly convoluted loop conformation are all *trans*. Unlike CsA, with just one ordered water molecule in the crystal structure, the structures of both CsH forms are heavily solvated, with eight and seven water molecules, respectively. Of the seven solvation water molecules in CsH form II, O1W is extremely well ordered, as judged by the refined anisotropic displacement parameters. Consideration of its interactions with neighboring atoms rules out the possibility that this could be a coordinated Mg^{2+} cation, which implies that these cations improve crystal ordering without being incorporated into the structure itself.

Here we describe the analysis of CsH form II by neutron diffraction. The positions of all hydrogen atoms in the peptide and solvent molecules were determined by crystallographic refinement.

11.10.2 Experimental

Highly purified cyclosporin H samples were supplied by Sandoz–Novartis, Basle, and crystals of CsH form-II were grown over twenty-one days at −20°C from methanol in the presence of magnesium perchlorate in partially sealed glass vials. Magnesium perchlorate was observed to extend the resolution of the X-ray diffraction pattern and to have a stabilizing effect on the structure, especially the long MeBmt-1 side chain, which is considerably disordered in the absence of the perchlorate. The crystals disintegrate spontaneously on exposure to air or water. For this reason it was not possible to deuterate the sample, unlike concanavalin A discussed above.

Neutron Data Collection and Processing
A crystal of cyclosporin H with approximate dimensions 0.5, 0.5, 0.3 mm was dipped in Fomblin oil, wrapped in thin aluminum foil, mounted on a thin V-pin, and rapidly cooled to 20 K in a cryo-refrigerator. Data were collected on VIVALDI. Eight Laue diffraction patterns were collected on a cylindrical image-plate detector at 10–20° intervals in a rotation of the crystal perpendicular to the incident beam. The crystal was held stationary during each 7-h Laue exposure, and then rotated to the next Laue position where it was held stationary again. The reflections were indexed using the program LAUEGEN and integrated using the program ARGONNE_BOXES, which is based on a two-dimensional implementation of the three-dimensional minimum $\sigma(I)/I$ algorithm [31]. Correction for absorption was unnecessary owing to the small nearly isotropic sample volume. The integrated reflections were wavelength normalized and scaled using the program LSCALE. A total of 9222 reflections was recorded of which 2849 were independent, resulting in 71.8% overall completeness for the resolution range 9.7–1.05 Å. Shell-wise merging and completeness statistics were computed with SCALA. Five percent (123) of the reflections were segregated for R_{free} calculations in order to monitor the refinement and help avoid the risk of over-fitting the data. Data collection, processing, and refinement statistics are presented in Table 11.6.

Since only the ratios between unit-cell dimensions could be accurately determined using the white beam Laue technique, the cell dimensions obtained by monochromatic X-ray diffraction at 298 K were used to index the neutron data. The crystal displayed anisotropic contraction with cooling, and it was necessary to refine the axis-length ratios: with the a axis held constant at 17.4 Å, the length of the c axis decreased by 3% from 23.2 to 22.4 Å. The unit cell length esd values from monochromatic X-ray measurement at room temperature were used for analysis.

11.10.3 Structure Refinement

Refinement against $|F|^2$ was performed using the Windows version of SHELXL-97. Initial atomic positions, including riding hydrogen atoms, were obtained from the results of the earlier X-ray structure, to which we have referred already. Owing to the relatively low data/parameter ratio, the refinement protocol was based on macromolecular refinement techniques, starting with a rigid-body refinement, then successively easing the restraints after each round of refinement and rebuilding, computing R_{free} on $|F|^2$at each step to monitor over-fitting of the data. In order to compensate for the change in unit-cell parameters relative to those at room temperature, the AFIX 9 command was used in the initial refinement cycle to model a "breathing" rigid-body fit. This initial refinement cycle with only 226 parameters resulted in an agreement factor of $R(|F|^2)$ of 28% and an $R_{\text{free}}(|F|^2)$ of 34%. Inspection of the initial nuclear density map showed well-resolved nuclear density for all atoms in the cyclic peptide, including clear nuclear density for a methyl rotor at residue 4, which had been modeled in the wrong conformation in the X-ray structure. The density for the hydrogen atoms on

Table 11.6 Crystal and neutron structure refinement data for CsH-II

Empirical formula	$C_{62}H_{123}N_{11}O_{18}$
M_r	1309.00
Temperature (K)	20(2)
Neutron wavelength (Å)	1.2–2.6
Crystal system	Orthorhombic
Space group	$P2_12_12_1$
Unit cell dimensions (Å)	$a = 17.392(2)$ $b = 19.3729(10)$ $c = 22.437(3)$
Volume (Å^3)	7559.6(14)
Z	4
Resolution range (last shell) (Å)	9.69–1.05(1.11–1.05)
R_{merge}	0.109(0.112)
*R*meas (all *I*+ and *I*−)	0.124(0.130)
Rpim (all *I*+ and *I*−)	0.057(0.064)
Total number of observations	9184(857)
Total number unique	2849(309)
Mean($(I)/\sigma$)	9.7(7.2)
Completeness	71.8(55.5)
Multiplicity	3.2(2.8)
D_c/Mg (m^{-3})	0.288
F(000)	160
Crystal size (mm)	0.5, 0.5, 0.5
Index ranges	$0 \le h \le 16,\ \ 0 \le k \le 18, 0 \le l \le 21$
Reflections collected	9222
Independent reflections	2849
Reflections used for SHELX	2726
R_{int}	0.1140
Overall completeness (last shell)	71.8%(55.5%)
Refinement method	Full-matrix least-squares on $\|F\|^2$
Data/restraints/parameters	2726/998/1303
Goodness-of-fit on $\|F\|^2$	1.572
Final *R* indices [$I > 2\sigma(I)$]	$R_1 = 0.1222$, $wR_2 = 0.2906$
R indices (all data)	$R_1 = 0.1382$, $wR_2 = 0.2988$

some solvent molecules was less clear, and ambiguous hydrogen atoms were deleted during this round of rebuilding. In the second round of least-squares refinement, the cyclic molecule was fitted as twelve rigid peptides and seven rigid water molecules.

Constraints were replaced with soft restraints as refinement progressed; finally, many of the restraints were removed entirely. Default SHELXL weights were employed for restraints, except for DELU (0.0001) and ISOR (0.005–0.01). Several common distances and angles were restrained to refined FVAR parameters. In the final cycle of refinement, these were: methyl C–H, amide N–H, water O–H, carbon C–H, C–C, N–CA and C=O bond distances; methyl H–C–H and water H–O–H angles. Releasing these restraints caused the $R_{1,free}$ index to increase from 0.168 to 0.183 with only modest diminishment of R_1, so the restraints were retained. Refinement statistics are listed in Table 11.6.

After completion of the refinement, each water molecule was omitted in turn for the calculation of least-squares water-omit maps. Every water hydrogen atom reappeared in its simulated annealing omit map with negative density greater in magnitude than 3σ in the $F_o - |F|_c$ nuclear density map,

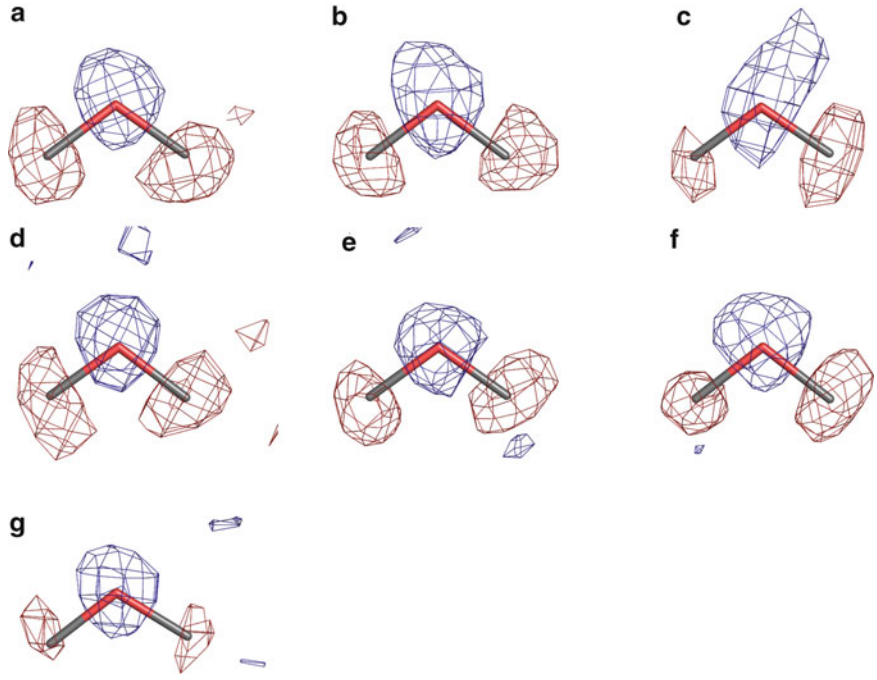

Fig. 11.18 (**a**–**g**) Mosiac of the water molecules in CsH in the "water-omit-refinement" $F_o - |F_c|$ nuclear difference density. Nuclear density is contoured at 3σ (blue) and -3σ (red)

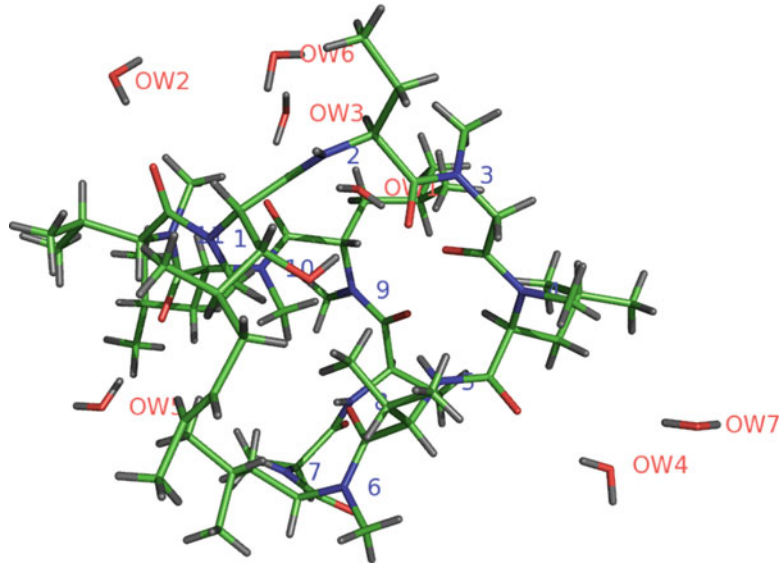

Fig. 11.19 View of CsH neutron structure

Fig. 11.18a–g. Figure 11.19 shows a view of the neutron structure. The final maps and ellipsoid plots were of high quality, Fig. 11.20.

Cyclosporin H-II with co-crystallized water has 217 atoms. With full positional and anisotropic thermal displacement parameters for all non-hydrogen atoms (the U values for some methyl hydrogen

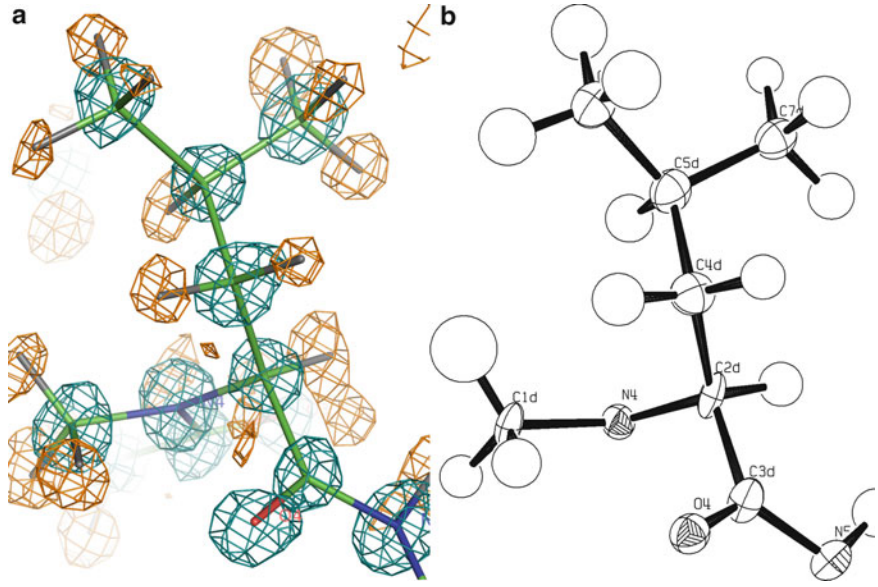

Fig. 11.20 (**a**) $2F_o - |F_c|$ nuclear density for residue 4 of CsH-II is shown to display the map quality. Positive density at the 2σ level is shown in teal, at -2σ in orange. (**b**) An ORTEP plot with ellipsoids shown at the 50 % confidence level. The hydrogen atoms are displayed with the radii proportional to refined U values

atoms were constrained to 1.5 times that of their carbon atom), the number of refined parameters in the final refinement cycle totaled 1303. With 2849 independent reflections and 217 atoms, the resulting data/atom ratio was 13.1 with a data/parameter ratio of 2.2. A total of 998 restraints was used for refinement: 185 to restrain chemically comparable bonds to common lengths, 73 to restrain angles, and 740 to restrain anisotropic thermal displacement ellipsoids. Refined bond lengths and angles generally compared well with those from the X-ray refinement, except that the C–H, N–H, and O–H bonds refined to larger values. Least-squares refinement of all atomic coordinates and anisotropic temperature factors resulted in a final agreement factor of $R_1(F^2) = 0.122$ for 2191 independent reflections with $F > 4\sigma(F)$. Relevant crystallographic data are summarized in Table 11.6. The unconventional nomenclature for atom labeling reflects the presence of D-peptides and several non-standard amino acids; atom naming follows that established in the X-ray structure analysis of cyclosporin H-II.

11.10.4 Description of the Neutron Structure and Comparison with the X-Ray Structure

The overall structure of CsH-II is a saddle-shaped, cyclic undecapeptide, Fig. 11.17a, b; the peptide sequence of CsH is (L)Bmt-(L)Abu-Sar-(L)MeLeu-(L)Val-(L)MeLeu-(L)Ala-(D)Ala-(L)MeLeu-(L)MeLeu-(D)MeVal. There are several non-standard amino acids in the polypeptide, including seven residues with methylated amide nitrogen atoms. Position 1 is assigned to the amino acid with the longest unbranched side chain, L-MeBMT. Position 2 is L-Abu. The amide nitrogen atoms at residues 1, 3, 4, 6, 8, 9, 10, and 11 are methylated. Residues 8 and 11 have the D-configuration at the α-C position (chiral inversion relative to the usual L-amino acid configuration). While six of the seven water molecules make at least one hydrogen bond with the peptide chain, Fig. 11.18a–g, water molecule seven does not interact directly with cyclosporin H, and may thus be described as occupying

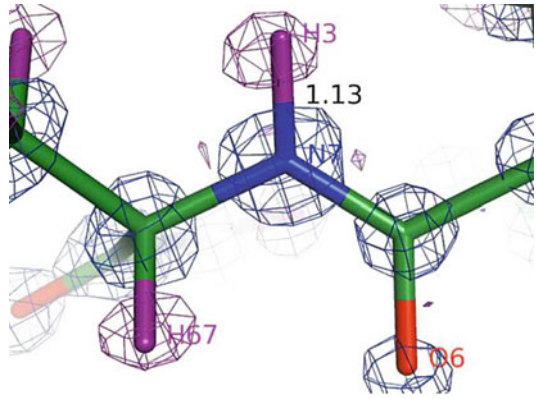

Fig. 11.21 The refined NH bond lengths in the neutron structure: average 1.135 Å compared with 0.86 Å in the X-ray structure

the second hydration sphere. Not coincidentally, the oxygen atom of water molecule seven exhibits the largest thermal motion and weakest nuclear density of all the water oxygen atoms, Fig. 11.18g.

The room temperature X-ray and cryo-neutron structures were superposed by the program LSQKAB, using the α-carbon atoms for alignment, Fig. 11.21; individual atom-by-atom displacements were computed with Perl Script. The average displacement for the 11 α-carbon atoms is 0.11 Å; for all peptide non-hydrogen atoms, the average displacement is 0.15 Å; for all water oxygen atoms, it is 0.16 Å. For all peptide hydrogen atoms, the average displacement is 0.27 Å; for water hydrogen atoms, it is 0.26 Å. The shifts are not anisotropic, that is, they do not correspond to shifts along the contracted cell axis. As neutrons are scattered by nuclei rather than electron clouds, the C–H, N–H, and O–H bond lengths are generally 0.14, 0.28, and 0.05 Å, respectively, longer than in the X-ray structure, Fig. 11.19, the largest difference being 0.56 Å at HW42, water molecule four.

There are minor differences in hydrogen atom positions at solvent sites 3, 4, 6, and 7.

The maximum atomic displacements between the X-ray structure and the neutron structure arose for the methyl hydrogen atoms of the amide nitrogen atom of residue 4. This methyl rotor had been misoriented by 60° in the X-ray structure determination. As would be expected, the hydrogen bonds found are consistent for both the X-ray and the neutron analyses. That is, all of the hydrogen bonds determined in the neutron study were also recognized in the X-ray structure. As in the X-ray structure, there is no indication of Mg^{2+} ions in the neutron structure, and it may be concluded that the presence of these ions in the crystallization medium merely serves to aid the crystallization process. This conclusion is supported by the distinct negative nuclear density for hydrogen atoms obtained in water-omit maps for every water molecule in the neutron structure analysis.

11.10.5 Conclusion

The complete atomic structure of cyclosporin H form II has been determined by single-crystal neutron diffraction. The relatively low data/parameter ratio required a mixed refinement strategy, similar to that employed in protein crystallography, Sect. 11.8. The unambiguous determination of all hydrogen atom positions completes the high-resolution single-crystal structure of cyclosporin H form II. The water hydrogen bonding interactions have now been directly determined, confirming that hydrogen bonding patterns inferred from X-ray refinement were essentially correct, but with minor differences, especially in the positions of hydrogen atoms on the solvent molecules. The refined neutron structure is illustrated in Figs. 11.22 and 11.23.

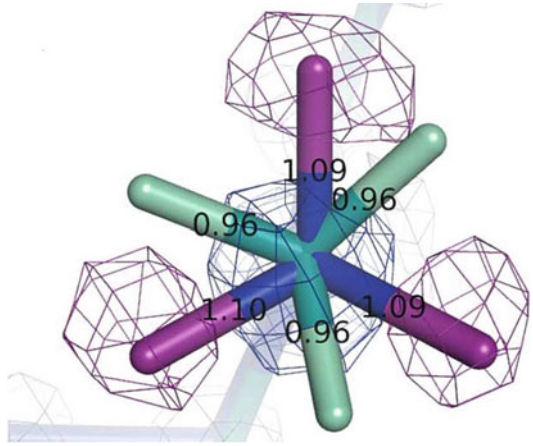

Fig. 11.22 Neutron data allowed correction of a CH_3 group orientation at residue 4. X-ray structure is shown in teal and green. Neutron structure in blue (C atoms and 2σ nuclear density) and purple (H atoms and –2σ nuclear density). C–H bond lengths refined to larger values in the neutron structure.

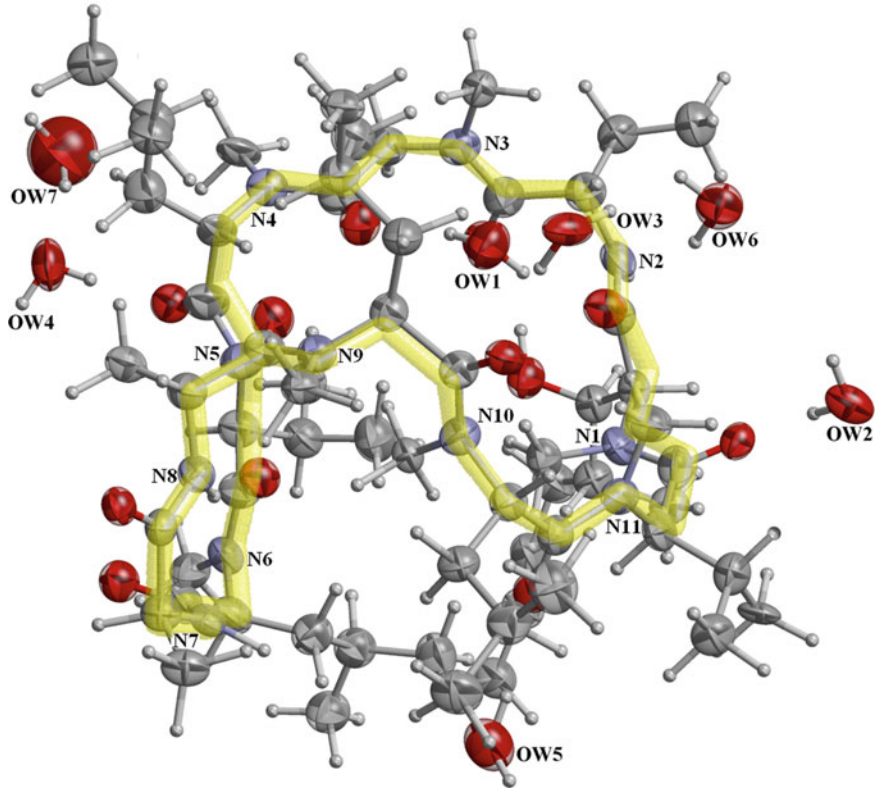

Fig. 11.23 CsH neutron structure showing the seven water molecules and trace of the main chain N1–N11. All water hydrogen atoms were determined experimentally. Thermal ellipsoids are plotted at 85% probability. The drawing was made with ORTEP-III/RASTER as implemented in the program suite WinGX and generated by ORTEP-3 for Windows. The main chain trace was drawn by RASMOL and inserted independently

11.11 Problems

11.1. A neutron beam has a wavelength spread of 1.0–2.0 Å. The beam is not quite parallel, the angular divergence being $\pm 0.25^\circ$ from the ideal path. The beam is monochromatized with a single crystal of lead (cubic, $a = 4.954$ Å) by reflection from the (111) face. (a) At what angle should the (111) planes be set so as to give a wavelength of 1.25 Å? (b) What would be the approximate spread of wavelength in the monochromatized beam?

11.2. Sodium hydride has the sodium chloride structure type, with $a = 4.88$ Å, Na^+ at 0, 0, 0, and H^- at 0, 0, 1/2. Using the data below, calculate F(111) and F(220) for NaH and NaD, for both X-rays and neutrons; the temperature factor may be neglected for the X-ray case. First, formulate a simplified structure factor equation for the calculation.

$f_{Na+}(111)$	8.1	$\beta_{Na^+}Z$	0.35
$f_{H^-/D^-}(111)$	0.38	$\beta_{H^-}Z$	−0.37
$f_{Na^+}(220)$	6.7	$\beta_{D^-}Z$	0.67
$f_{H^-/D^-}(220)$	0.21		

11.3. When using the VIVALDI instrument to collect neutron diffraction data, why might it be necessary first to undertake preliminary studies of a crystal using X-ray diffraction?

11.4. The neutron spallation beam at ORNL is extremely powerful. Why is it recommended that users should supply crystals as large as 1 mm^3, whereas VIVALDI users can frequently collect excellent neutron diffraction data on much smaller crystals?

11.5. Calculate the wavelength of a neutron beam having an associated temperature $T = 273$ K.

11.6. Use RASMOL to reproduce as closely as possible Fig. 11.12 showing the Mn coordination sphere in Concanavalin A. Table 8.4 may also be useful.

Suggested strategy:

1. Download the program RASMOL.
2. Go to the PDB website and download PDB file 1scs.
3. Read the file 1scs using RASMOL.
4. Maximize the display.
5. Locate the independent command display for RASMOL which will be at the bottom of your screen.
6. Enter the following commands using this display:

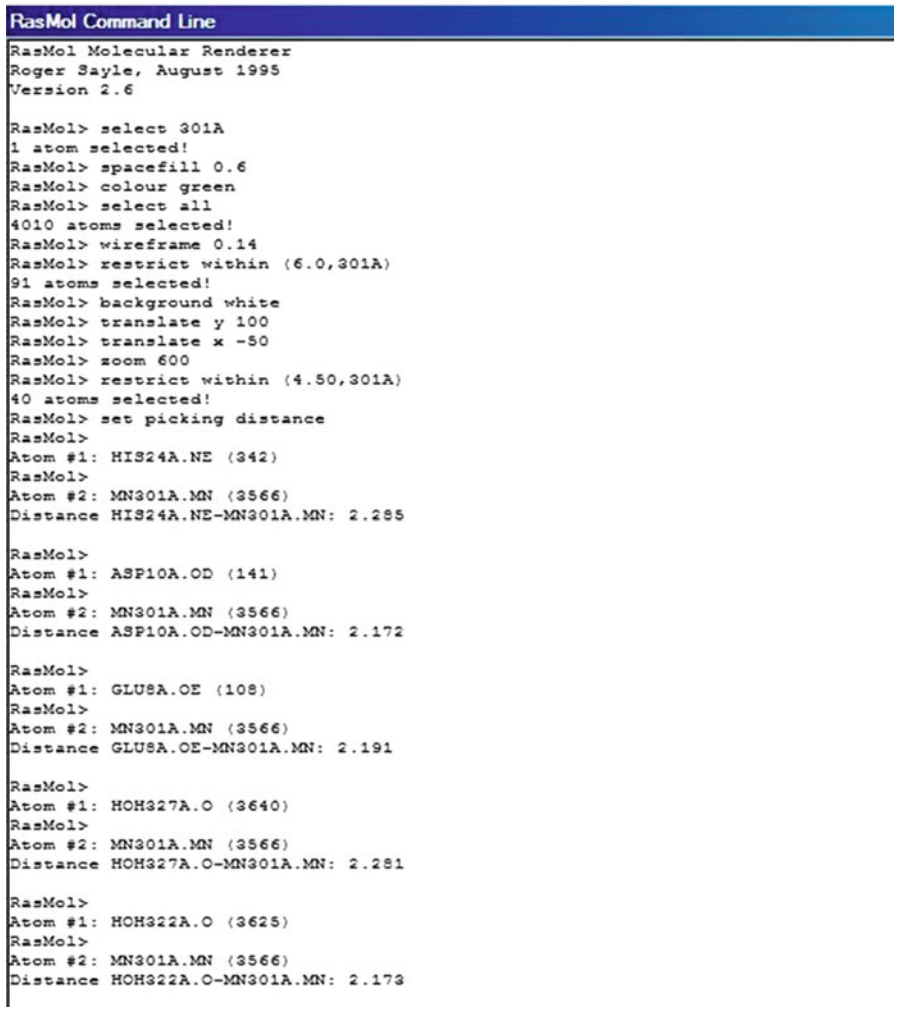

References

1. Myles DAA (2006) Curr Opin Struct Biol 16:630
2. Helliwell JR et al (1989) J Appl Crystallogr 22:483–497
3. Cruickshank DW, Helliwell JR, Moffat K (1987) Acta Crystallogr A43:656
4. Cruickshank DW, Helliwell JR, Moffat K (1991) Acta Crystallogr A47:352
5. Ren Z et al (1999) J Synch Rad 6:891
6. http://www.ncnr.nist.gov/resources/n-lengths/ele ments/h.html
7. Neutron News, 3:29 (1992)
8. http://www.ncnr.nist.gov/resources/n-lengths
9. Sheldrick GM (2008) Acta Crystallogr A64:112
10. McIntyre G et al (2006) Phys B Condens Matter 385:1055
11. Wilkinson C et al (2002) Neutron News 13:37
12. Teixera SC et al (2008) Chem Phys 345:133
13. http://www.ill.eu/html/about/movies/experiments/vivaldi- laue-diffraction
14. http://neutrons.ornl.gov/facilities/

15. http://neutrons.ornl.gov/instruments/SNS/MaNDi/
16. http://www.b2bfreezone.com/product-search/deut erated-compounds.htm
17. http://www.patentstorm.us/patents/5733984/descrip tion.html
18. http://www.ansto.gov.au/research/bragg_institute/facilities/molecular_deuteration
19. ILL-EMBL Deuteration Laboratory, Partnership for structural biology, Grenoble, France
20. Petit-Haertlein I, Blakeley MP, Howard E, Hazemann I, Mitschler A, Haertlein M, Podjarny A (2009) Acta Crystallogr F Struct Biol Cryst Commun 1:406
21. Palmer RA et al (2001) Acta Crystallogr B57:339 and references therein
22. http://www.ccp4.ac.uk/html/pointless.html
23. Habash J et al (2000) Acta Crystallogr D56:541 and references therein
24. Kalb (Gilboa) AJ et al (1999) In: Sigel A, Sigel H (eds) Metal ions in biological systems: manganese and its role in biological processes.vol 37. Marcel Dekker, New York, p 279
25. Wlodawer A (1982) Prog Biophys Mol Biol 40:115
26. Emmerich C et al (1994) Acta Crystallogr D50:749
27. Collaborative Computational Project, Number 4 [CCP4] (1994)
28. Wlodawer A (1982) loc cit
29. Potter BS (2001) PhD Thesis, University of London
30. Brian Potter BS, Palmer RA, Withnall R, Jenkins T, Chowdhry BZ (2003) Org Biomol Chem 1:1466 and references therein
31. Wilkinson C et al (1988) J Appl Crystallogr B21:47
32. Gardberg A, Potter B, Palmer R, Myles D, McDonald G (2011) J Chem Cryst 41:470 and references therein

Bibliography: Neutron Diffraction

Bacon GE (1975) Neutron diffraction, 3rd edn. Clarendon Press, Oxford
Bacon GE (1963) Applications of neutron diffraction in chemistry. Pergamon Press, New York
Niimura N, Podjarny A (2011) Neutron protein crystallography, I. U. Cr. Monograph (Book 25)
Sherwood D, Cooper J (2011) Crystals, X-rays and protein crystallography (chapter 16). OUP, Oxford
Wilson CC (2000) Single crystal neutron diffraction from molecular materials. World Scientific, Singapore. Onlinelibrary.wiley.com/doi/10.1107/S01087673010 05980/abstract

Structure of Proteins

Branden C, Tooze J (1999) Introduction to protein structure, 2nd edn. Garland Publishing, New York
Blow DM (2002) Outline of crystallography for biologists. OUP, Oxford
Palmer RA (2000) X-ray crystallographic studies of protein-ligand interactions in protein-ligand interactions (chapter 12). In: Chowdhury B, Harding S (eds) Practical approach series. OUP, England

Proteins

Chayen NE, Helliwell JR, Snell EH (2010) Macromolecular crystallization and crystal perfection. Oxford University Press, Oxford